IJOER
RESEARCH JOURNAL

International Journal
of
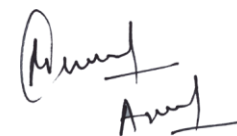## Engineering Research & Science

Preface

We would like to present, with great pleasure, the inaugural volume-6, Issue-9, September 2020, of a scholarly journal, *International Journal of Engineering Research & Science*. This journal is part of the AD Publications series *in the field of Engineering, Mathematics, Physics, Chemistry and science Research Development*, and is devoted to the gamut of Engineering and Science issues, from theoretical aspects to application-dependent studies and the validation of emerging technologies.

This journal was envisioned and founded to represent the growing needs of Engineering and Science as an emerging and increasingly vital field, now widely recognized as an integral part of scientific and technical investigations. Its mission is to become a voice of the Engineering and Science community, addressing researchers and practitioners in below areas

Chemical Engineering	
Biomolecular Engineering	Materials Engineering
Molecular Engineering	Process Engineering
Corrosion Engineering	
Civil Engineering	
Environmental Engineering	Geotechnical Engineering
Structural Engineering	Mining Engineering
Transport Engineering	Water resources Engineering
Electrical Engineering	
Power System Engineering	Optical Engineering
Mechanical Engineering	
Acoustical Engineering	Manufacturing Engineering
Optomechanical Engineering	Thermal Engineering
Power plant Engineering	Energy Engineering
Sports Engineering	Vehicle Engineering
Software Engineering	
Computer-aided Engineering	Cryptographic Engineering
Teletraffic Engineering	Web Engineering
System Engineering	
Mathematics	
Arithmetic	Algebra
Number theory	Field theory and polynomials
Analysis	Combinatorics
Geometry and topology	Topology
Probability and Statistics	Computational Science
Physical Science	Operational Research
Physics	
Nuclear and particle physics	Atomic, molecular, and optical physics
Condensed matter physics	Astrophysics
Applied Physics	Modern physics
Philosophy	Core theories

Chemistry	
Analytical chemistry	Biochemistry
Inorganic chemistry	Materials chemistry
Neurochemistry	Nuclear chemistry
Organic chemistry	Physical chemistry
Other Engineering Areas	
Aerospace Engineering	Agricultural Engineering
Applied Engineering	Biomedical Engineering
Biological Engineering	Building services Engineering
Energy Engineering	Railway Engineering
Industrial Engineering	Mechatronics Engineering
Management Engineering	Military Engineering
Petroleum Engineering	Nuclear Engineering
Textile Engineering	Nano Engineering
Algorithm and Computational Complexity	Artificial Intelligence
Electronics & Communication Engineering	Image Processing
Information Retrieval	Low Power VLSI Design
Neural Networks	Plastic Engineering

Each article in this issue provides an example of a concrete industrial application or a case study of the presented methodology to amplify the impact of the contribution. We are very thankful to everybody within that community who supported the idea of creating a new Research with IJOER. We are certain that this issue will be followed by many others, reporting new developments in the Engineering and Science field. This issue would not have been possible without the great support of the Reviewer, Editorial Board members and also with our Advisory Board Members, and we would like to express our sincere thanks to all of them. We would also like to express our gratitude to the editorial staff of AD Publications, who supported us at every stage of the project. It is our hope that this fine collection of articles will be a valuable resource for *IJOER* readers and will stimulate further research into the vibrant area of Engineering and Science Research.

Mukesh Arora

(Chief Editor)

Dr. Mohamed Abdel Fatah Ashabrawy Moustafa

PhD. in Computer Science - Faculty of Science - Suez Canal University University, 2010, Egypt.

Assistant Professor Computer Science, Prince Sattam bin AbdulAziz University ALkharj, KSA.

Dr. Heba Mahmoud Mohamed Afify

Ph.D degree of philosophy in Biomedical Engineering, Cairo University, Egypt worked as Assistant Professor at MTI University.

Dr. Aurora Angela Pisano

Ph.D. in Civil Engineering, Currently Serving as Associate Professor of Solid and Structural Mechanics (scientific discipline area nationally denoted as ICAR/08"–"Scienza delle Costruzioni"), University Mediterranea of Reggio Calabria, Italy.

Dr. Faizullah Mahar

Associate Professor in Department of Electrical Engineering, Balochistan University Engineering & Technology Khuzdar. He is PhD (Electronic Engineering) from IQRA University, Defense View,Karachi, Pakistan.

Dr. S. Kannadhasan

Ph.D (Smart Antennas), M.E (Communication Systems), M.B.A (Human Resources).

Dr. Christo Ananth

Ph.D. Co-operative Networks, M.E. Applied Electronics, B.E Electronics & Communication Engineering Working as Associate Professor, Lecturer and Faculty Advisor/ Department of Electronics & Communication Engineering in Francis Xavier Engineering College, Tirunelveli.

Dr. S.R.Boselin Prabhu

Ph.D, Wireless Sensor Networks, M.E. Network Engineering, Excellent Professional Achievement Award Winner from Society of Professional Engineers Biography Included in Marquis Who's Who in the World (Academic Year 2015 and 2016). Currently Serving as Assistant Professor in the department of ECE in SVS College of Engineering, Coimbatore.

Dr. Maheshwar Shrestha

Postdoctoral Research Fellow in DEPT. OF ELE ENGG & COMP SCI, SDSU, Brookings, SD Ph.D, M.Sc. in Electrical Engineering from SOUTH DAKOTA STATE UNIVERSITY, Brookings, SD.

Zairi Ismael Rizman

Senior Lecturer, Faculty of Electrical Engineering, Universiti Teknologi MARA (UiTM) (Terengganu) Malaysia Master (Science) in Microelectronics (2005), Universiti Kebangsaan Malaysia (UKM), Malaysia. Bachelor (Hons.) and Diploma in Electrical Engineering (Communication) (2002), UiTM Shah Alam, Malaysia

Dr. D. Amaranatha Reddy

Ph.D.(Postdocteral Fellow,Pusan National University, South Korea), M.Sc., B.Sc. : Physics.

Dr. Dibya Prakash Rai

Post Doctoral Fellow (PDF), M.Sc.,B.Sc., Working as Assistant Professor in Department of Physics in Pachhuncga University College, Mizoram, India.

Dr. Pankaj Kumar Pal

Ph.D R/S, ECE Deptt., IIT-Roorkee.

Dr. P. Thangam

BE(Computer Hardware & Software), ME(CSE), PhD in Information & Communication Engineering, currently serving as Associate Professor in the Department of Computer Science and Engineering of Coimbatore Institute of Engineering and Technology.

Dr. Pradeep K. Sharma

PhD., M.Phil, M.Sc, B.Sc, in Physics, MBA in System Management, Presently working as Provost and Associate Professor & Head of Department for Physics in University of Engineering & Management, Jaipur.

Dr. R. Devi Priya

Ph.D (CSE),Anna University Chennai in 2013, M.E, B.E (CSE) from Kongu Engineering College, currently working in the Department of Computer Science and Engineering in Kongu Engineering College, Tamil Nadu, India.

Dr. Sandeep

Post-doctoral fellow, Principal Investigator, Young Scientist Scheme Project (DST-SERB), Department of Physics, Mizoram University, Aizawl Mizoram, India- 796001.

Mr. Abilash

MTech in VLSI, BTech in Electronics & Telecommunication engineering through A.M.I.E.T.E from Central Electronics Engineering Research Institute (C.E.E.R.I) Pilani, Industrial Electronics from ATI-EPI Hyderabad, IEEE course in Mechatronics, CSHAM from Birla Institute Of Professional Studies.

Mr. Varun Shukla

M.Tech in ECE from RGPV (Awarded with silver Medal By President of India), Assistant Professor, Dept. of ECE, PSIT, Kanpur.

Mr. Shrikant Harle

Presently working as a Assistant Professor in Civil Engineering field of Prof. Ram Meghe College of Engineering and Management, Amravati. He was Senior Design Engineer (Larsen & Toubro Limited, India).

Table of Contents

Autogenous Yb:YAG laser disk welding domain of AA6061-T4 aluminium alloy

Ameth Faye[1], Yannick Balcaen[2], Loic Lacroix[3], Joel Alexis[4]

Université de Toulouse, LGP, ENIT/INPT, 47 av. d'Azereix, BP1629, 65016 Tarbes cedex, France

Abstract*— The aerospace industry is developing lighter, stronger and more heat- and corrosion-resistant components to reduce manufacturing costs and fuel consumption. To achieve this goal, laser welding represents a real opportunity to replace the riveting assemblies developed in the 1920s. In this article, we present our research to obtain the weldability domain of AA6061 aluminium alloy by autogenous disk laser welding. A systematic study of the samples butt-welded by X-ray and optical microscopy allowed us to determine the defects and the dimensions of the weld beads according to the process parameters. The data analysis with the CORICO software made it possible to determine the regression models considering the welding parameters in order to avoid the appearance of defects such as melt pool collapse, lack of penetration or hot cracking. A range of weldability was defined for power values between 2000 to 2500 W, welding speeds below 4m/min and focal diameters below 170 microns.*

Keywords*— aluminium alloy, laser welding, weldability domain.*

I.   INTRODUCTION

Since the beginning of the 21st century, the share of organic matrix composite materials has increased considerably in aircraft structures [1]. In order to remain competitive for the manufacture of new single-aisle aircraft, new metal alloys or new solutions for using these alloys will have to be developed. Concerning aluminium alloys, which remain key alloys for the aeronautical field, two solutions for joining by friction stir welding or laser welding seem promising to replace the riveting assemblies developed in the 1920s. These complementary processes result in weight savings by eliminating excess thickness or sealant and productivity gains [2–4].

Concerning more specifically laser welding, there are nowadays several laser sources such as CO_2 lasers or solid-state lasers (fiber or disc). CO_2 sources have been implemented faster in the industry because they were more powerful and cheaper. The advent of the new disc sources allows for higher quality, higher power and lower cost solid state laser beams [5,6]. In addition, their shorter wavelength compared to CO_2 lasers reduces reflection problems when welding alloys such as aluminium alloys [7]. Indeed, the physical and chemical characteristics of high-strength aluminium alloys lead to welding difficulties that must be considered in the welding procedures. The most frequently encountered problems are the difficulty to obtain sufficient penetration depths, correct bead geometries, weld beads without porosity and cracks. Insufficient penetration of the fusion zone is due to insufficient laser beam energy during welding. Geometrical defects such as undercut or incomplete fusion can be generated when welding speeds are too high [8]. Hot cracking occurs at the end of the solidification of the alloy when the dendritic skeleton is not sufficiently formed to resist deformation and the permeability of the liquid medium is very low. At this stage, the material has low strength and low ductility. In order to limit this susceptibility to hot cracking, Hu et al. propose to optimize welding parameters, to reduce thermal contraction stresses by preheating or by modifying the chemical composition of the molten bath with a filler metal [9]. The small porosities are due to the low miscibility of hydrogen in the solid state of aluminium alloys [10]. The presence of hydrogen in the liquid bath during welding is due to poor surface preparation [11]. Large porosities can also exist in welds. They result from instability of the keyhole during the welding phase [12]. The extent of these weld defects depends, among other things, on the welding parameters, hence the need to study the influence of each parameter on the characteristics of the weld [13]. In this study, the weldability range of AA6061-T4 alloy, without filler metal, was investigated using an Yb: YAG source.

II.   MATERIALS AND METHODS

2.1   Sample welding conditions

The samples were butt welded, without filler metal, using a 3. 3 kW Yb:YAG disc laser source on a TruLaser Cell 3000 five-axis laser machine. The emitted beam is guided by a 2-in-1 coaxial optical fiber. The focal diameter can therefore vary from 120 μm to 370 μm for the Core Fiber (CF) and from 450 μm to 750 μm for the Outer Fiber (OF). The power density is distributed in Gaussian form for the CF and annular for the OF [7,14]. The clamping system allows the samples to be maintained edge to edge, with precise positioning of the parting line (Fig. 1). The shielding gas on the reverse side sweeps along the entire length of the bead, in the opposite direction to the welding direction. The primary chamber is designed to contain the metal vapors from the weld bead under gas protection. The bottom of the secondary chamber consists of a copper reflector, which reflects the fraction of the beam that can possibly pass through the weld bead towards the wall of this chamber.
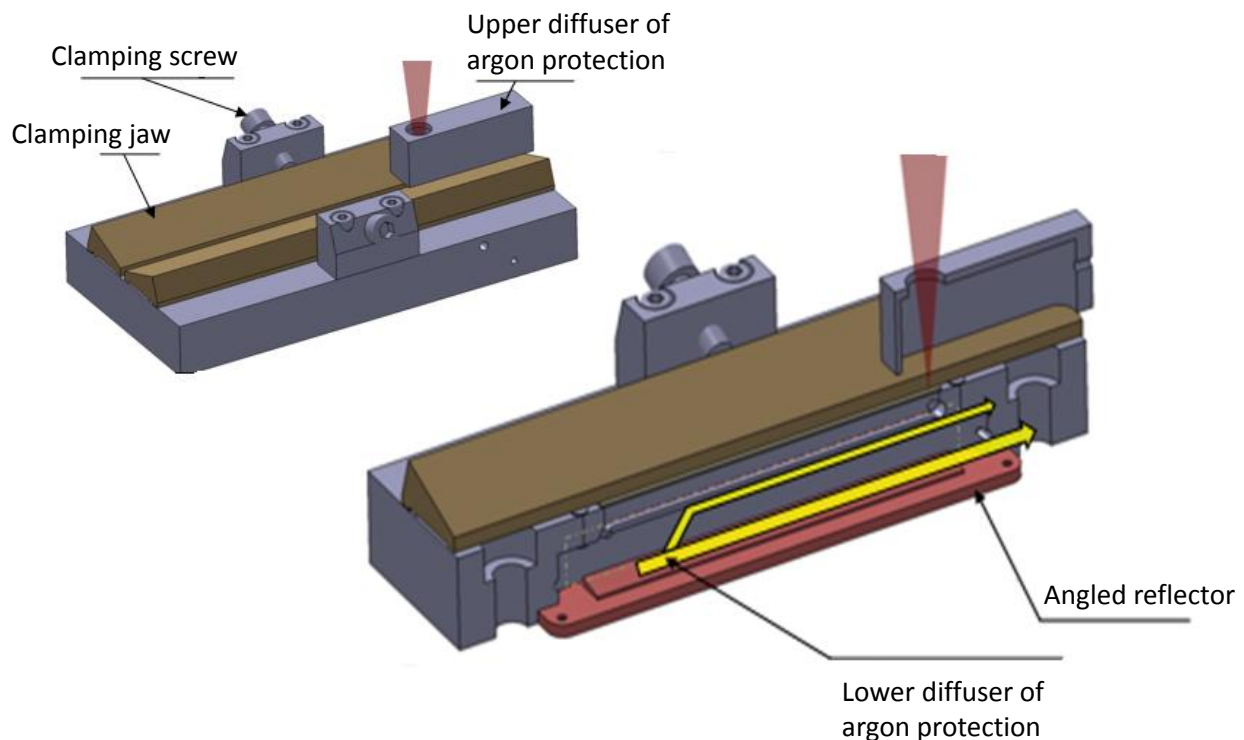
FIGURE 1: Experimental set-up to weld AA6061 aluminium alloy samples

The surface preparation followed before welding consists in mechanical stripping (sanding with P600 SiC paper) to renew the alumina layer, removing other hydroxide compounds that may form on the surface of the material. This step is followed by degreasing and cleaning of the surface of the part using acetone. The surface preparation aims to promote weldability but also to guarantee a good internal bead health (porosities, oxide inclusions). To make the preparation effective, the welding is carried out shortly (less than an hour) after preparation.

The study of the influence of parameters such as beam power, welding speed, the focal point diameter on the bead geometry, on the porosity and cracking was carried out for both fiber configurations (Table 1). In order to limit the number of samples while trying to obtain as much information as possible between process parameters and bead characteristics, experimental designs were generated for each fiber from the CORICO[TM] software[15]. 108 samples were welded for this study (36 with the OF and 72 with the CF). Other operating parameters are set such as the position of the focal point in relation to the sheet metal surface, the nature and flow rate of the gas for upper and lower weld protection or the surface preparation of the AA6061 sheet metal (Table 2).

TABLE 1
VARIABLE OPERATING PARAMETERS OF THE STUDY

Beam power (W)	500 to2500
Welding speed (m/min)	1 to 8
Focal diameter (µm)	120 to 370 (core fiber) 450 to 750 (outer fiber)

TABLE 2
FIXED PARAMETERS DURING THE WELDING OPERATION

Position of the focal point relative to upper the surface	Protective gas: Nature / gas flow rate	
	Upper protection	Lower protection
0. 3 mm	Argon / 40l/min	Argon / 20 l/min

2.2 Methods for characterizing welds

All the weld beads were first studied by non-destructive methods. Radiographic observations were carried out for the analysis of volume defects (porosities) or plane defects (cracks) using the Easytom RX Solution tomograph. The acquisition parameters used are a voltage of 115 kV and a current of 260 µA. These analyses were supplemented by metallographic observations in transverse section in order to determine the morphology and dimension of the welds as a function of the operating parameters. The validation of the beads is based on the acceptance criteria for welds of aluminium alloy parts defined by the NF L 06-395 2010. Based on these criteria, a weldability range of the 1mm-thick AA6061-T4 alloy welded with the Yb: YAG laser has been determined (Table 3).

TABLE 3
GEOMETRICAL CRITERIA FOR WELD SEAMS ACCORDING TO THE NF L06-395 2010 STANDARD.

Defect	Symbol	Dimensions (mm)	
Face width:	L	2	maxi
Face concavity:	-R	-0. 1	mini
Face reinforcement:	R	0. 3	maxi
Face undercut:	C	0. 15	maxi
Root width	l	1. 5	maxi
Root concavity:	-r	-0. 1	mini
Root reinforcement	r	0. 4	maxi
Root undercut	c	0. 1	maxi
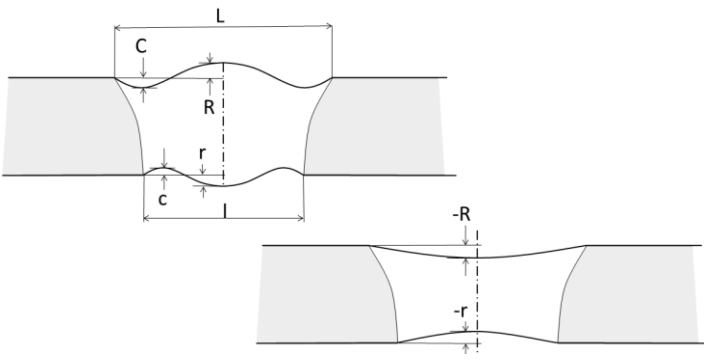
III.   RESULTS AND DISCUSSION

3.1   Weldability domain

3.1.1   Bath collapse and weld penetration

The collapse of the molten pool and the pronounced lack of penetration were observed by light microscopy on some beads (Fig. 2). Of the 108 samples, 39 weld beads showed a penetrating weld without melt pool collapse (36 with CF and 3 with OF). Collapse is generally observed when the power density of the laser beam is excessive ($>10^7$ W/cm^2) and/or the interaction time is greater than 5. 5 10^{-3}s. This defect is only encountered with the core fiber configuration, where power density levels are very high (up to 2 10^7 W/cm^2). In this case, it is preferable to decrease the beam power or increase the focal diameter. The lack of penetration is, on the contrary, usually caused by low beam power and/or high welding speed. The high thermal diffusivity of aluminium and its alloys as well as their high reflection due to the brightness of their surface favors these risks of fusion lack of the edges to be joined by preventing the necessary absorption of heat to melt the parts to be

welded. This defect type, mainly driven by the beam power density, strongly limits welding with the large fiber of the TruLaser Cell 3. 3 kW center where, due to the large focal diameter, the power density of the beam does not exceed 1. 5 10^6 W/cm^2. More than 91 % of the beads welded using outer fiber present penetration defect.
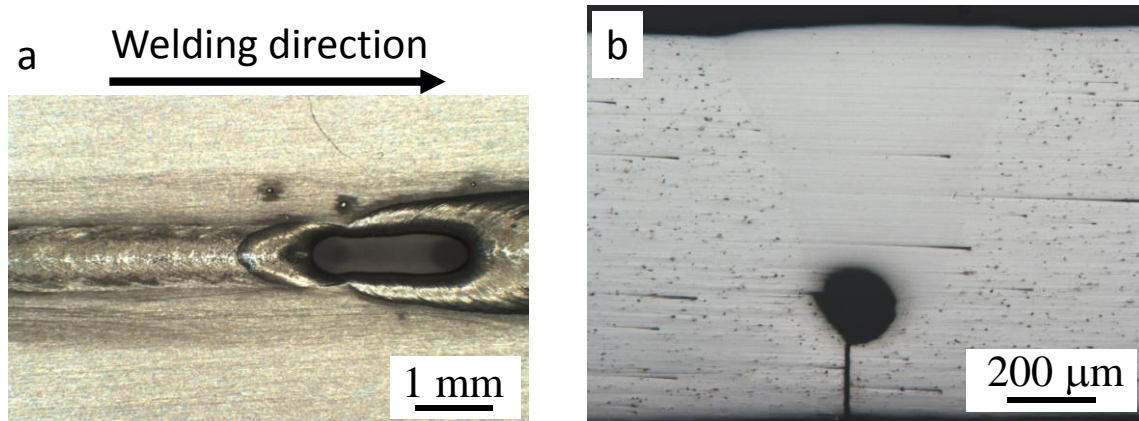
FIGURE 2: Optical observations with defects in the welds: (a) face view of molten pool collapse (P = 2000 W, V = 2. 75 m/min, Øf = 305 μm), (b) Cross section evidencing lack of penetration and associated root porosity (P = 2500 W, V = 4. 5 m/min,Øf = 600 μm)

Cords with both good penetration and no collapse were radiographed to investigate the possible presence of porosities and cracking.

3.1.2   Porosity and cracking

X-ray analysis revealed a few microporosities averaging about 60 μm in size in some welds (Fig. 2). However, no cracks or macroporosities were observed on the pre-selected welds for tomographic analysis. Optical microscopic observations of metallographic sections confirmed the presence of pores with a diameter of about 15 μm (Fig. 4a). Cracks were also observed in the fusion zone of the welds obtained with the outer fiber (Fig. 4b). The welding of AA6061 with the outer fiber is therefore limited by the lack of penetration and cracking. Nevertheless, the welds made with a small focal diameter (CF) are all free of cracking. As a reminder, according to the NF L 06-395 2010, no crack, whatever its size, is tolerable in a weld of an aluminium part. In conclusion, a range of weldability exists for AA6061 alloy by laser welding Yb:YAG without filler metal.
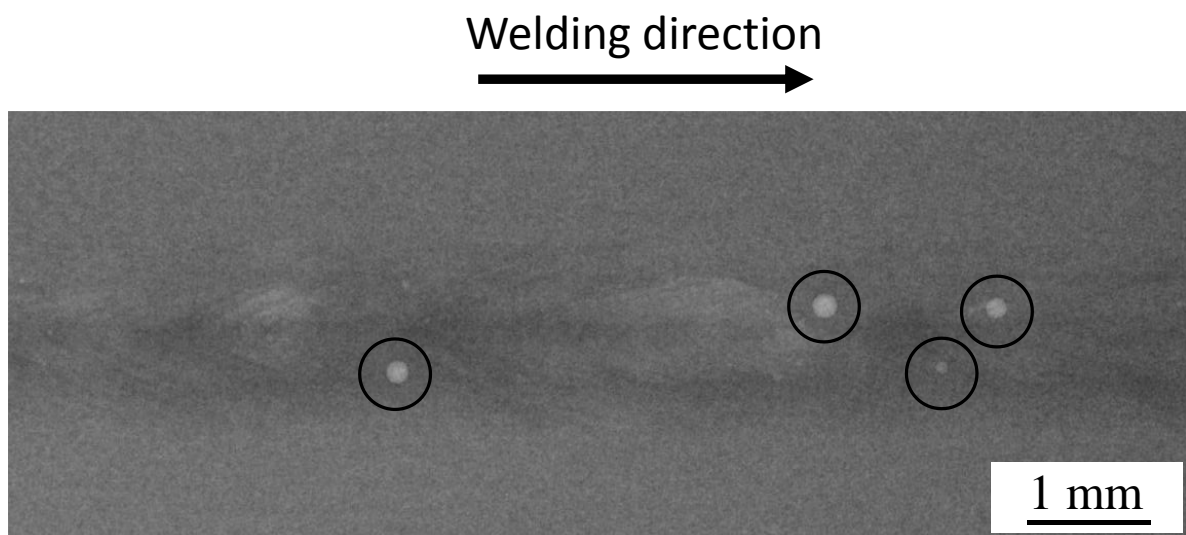
FIGURE 3: X-ray radiographic observation showing microporosities in the fusion zone of a weld (P = 2230 W, V = 3. 7 m/min, Øf = 153 μm)
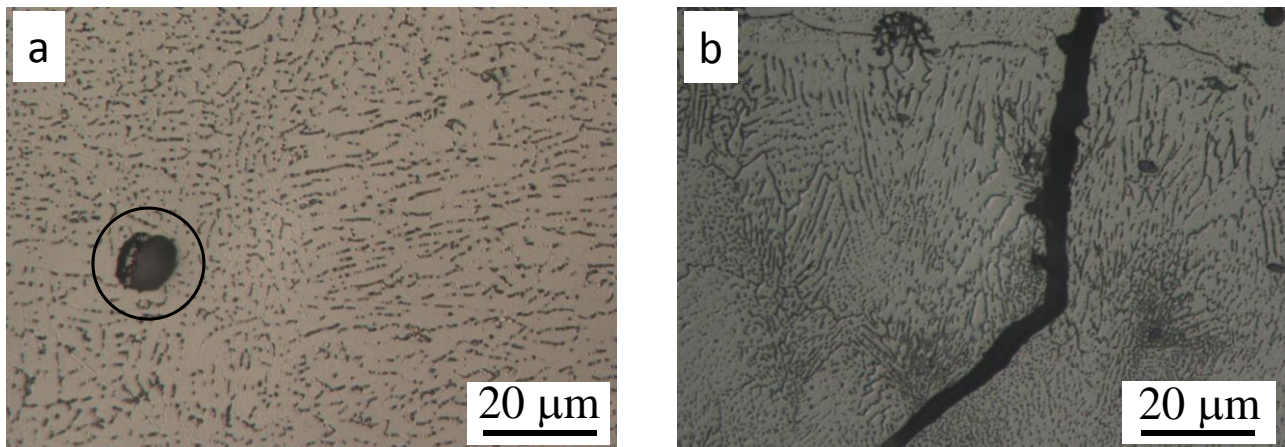
FIGURE 4: Optical micrographs showing (a) porosity (P = 2000 W, V = 2. 27 m/min, Øf = 134 μm) and (b) cracking in the fusion zone of a weld (P = 2500 W, V = 2. 5 m/min, Øf = 675 μm)

3.1.3   Geometry weld defects

Dimensional limits for specific common imperfections and shape dimensions in laser beam fusion welding are also measured to verify weld bead conformance. The figure 5 shows different shapes of weld beads in cross section. In spite of good penetration and the absence of porosity and cracking, geometrical defects may appear at the base or on the right side of the weld beads. Such defects generally constitute areas of crack initiation but also concentration of internal stresses that weaken the part. They are therefore prohibited. Approximately 23% of CF fiber specimens without porosities or cracks have a geometry defect. This weld cross-sectional irregularity is observed, in most cases, when the power density is greater than 10^6 W/cm^2 and the interaction time is less than $5 10^{-3}$ s. This corresponds to a range of high power and high welding speed leading to instability of the molten pool. This phenomenon is facilitated by the thermal properties of the alloy.
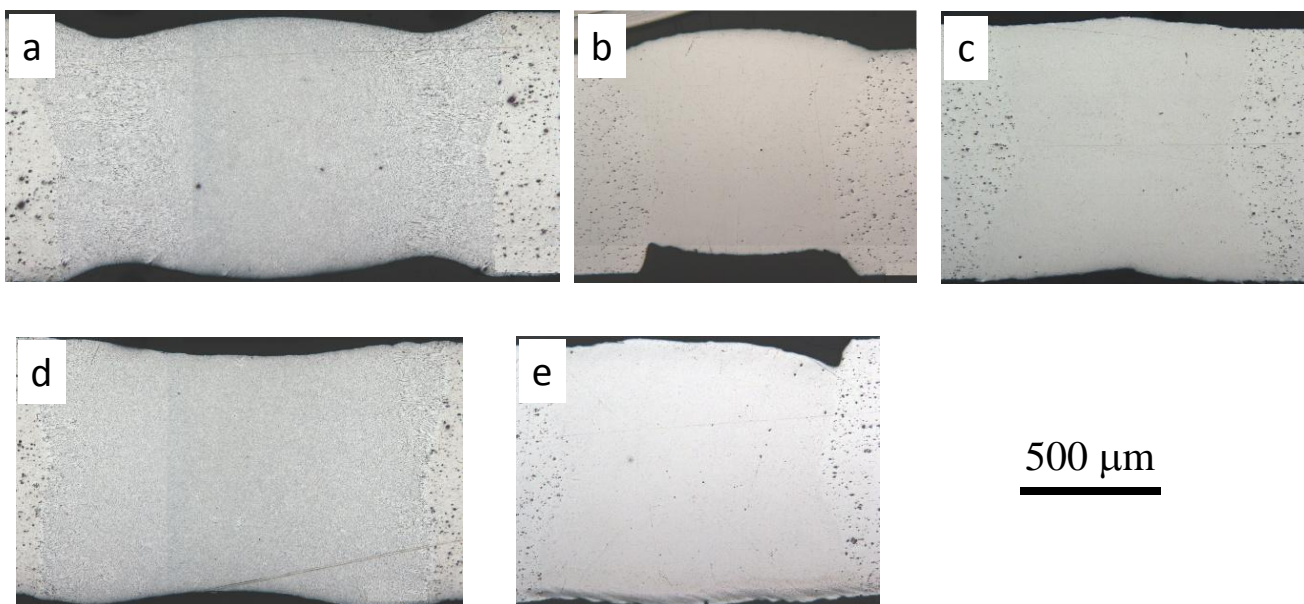
FIGURE 5: Non-conforming weld bead micrographs:(a) P = 900 W, V = 7. 05 m/min,Øf = 195μm, (b)P = 2500 W, V = 8 m/min, Øf = 370 μm, (c)P = 1000 W, V = 2. 75 m/min, Øf = 240 μm(d)1000 W, V = 6. 25m/min, Øf = 175 μm, (e)P = 2000 W,V = 8 m/min, Øf = 305 μm.

Among all the welded samples, only 26 were able to meet the above-mentioned standard requirements. This corresponds to slightly less than 25% of the full experimental design. The weldability range of the 1 mm thick alloy AA6061-T4 welded by laser beam Yb: YAG according to the criteria chosen in this study is shown in Figure 6. This weldability range is defined at power densities between $5 10^6$ and $2 10^7$ W/cm^2 and an interaction time lower than $6 10^{-3}$ s. Only the core fiber allows welding this alloy thanks to the high-power densities lJof the laser beam. Welding with the outerfiber is limited by penetration and hot cracking defects. Indeed, with the outerfiber, the power densities do not allow to melt the whole thickness of the part to be assembled, without generating excessively wide beads, presenting hot cracking.
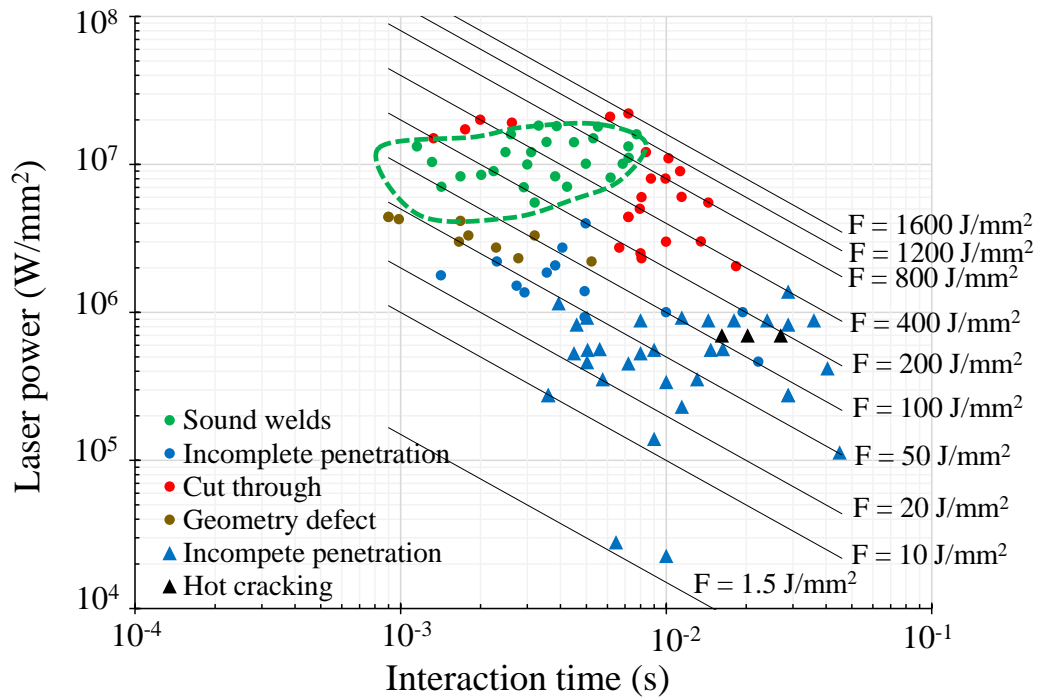
FIGURE 6: Weldability domain of AW6061-T4 welded by Yb: YAG laser

3.2   First order process parameters

The presentation of the weldability range as a function of power density and interaction time cannot be used directly to weld AA6061-T4 alloy. It is necessary to decouple each operating parameter (laser power, welding speed and diameter at the focal point) to determine their influence on the weldability criteria chosen in this study, i. e. penetration, bead geometry, melt pool collapse or cracking. To reach this objective, we determined the iconographic sphere of the correlations between the laser parameters and the weldability criteria (Fig. 7).
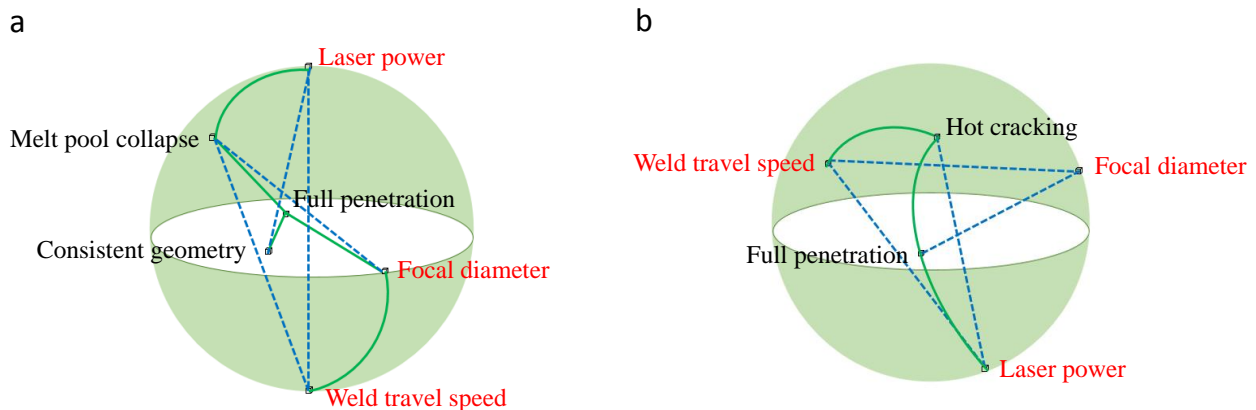
FIGURE 7: Iconographic correlation spheres for Yb: YAG laser welding of alloy AA6061-T4: (a) core fiber, (b) outer fiber

In the correlation iconography, solid lines indicate a positive correlation and dashed lines indicate a negative correlation. The smaller the distance between the factor and the response, the greater the contribution of that factor. For the welds obtained with the core fiber, only the power of the laser beam has a positive correlation with the collapse of the molten pool. In fact, an increase in the beam power leads to the difficulty of stabilizing the keyhole and therefore the possibility of having a melt bath collapse or incorrect geometry beads. An increase in welding speed reduces the susceptibility to melt pool collapse. An increase in focal diameter improves weld penetration. Indeed, the power density becomes excessive when the focal diameter is very small and under these conditions the molten pool collapse becomes almost inevitable. We can say that for laser welding with small fiber, every process parameter has a strong influence on welding problems such as melt pool collapse, lack of penetration and non-conformity of the bead geometry. For a good quality weld, an optimum choice of these

parameters seems to be necessary. For welds obtained with the outer fiber, a minimum power density is necessary to obtain sufficient penetration of the beads. This can be achieved mainly by increasing the beam power or by decreasing the focal point diameter. On the other hand, an increase in cord penetration is accompanied by the risk of hot cracking. This risk is increased with an increase in welding speed [16].

The response areas for obtaining a conformal weld bead with the core fiber are given in Figure 8. To obtain compliant weld beads, the process parameters must be within the following ranges: power between 2000 and 2500 W, focal diameter less than 170 μm and welding speed less than 4 m/min.
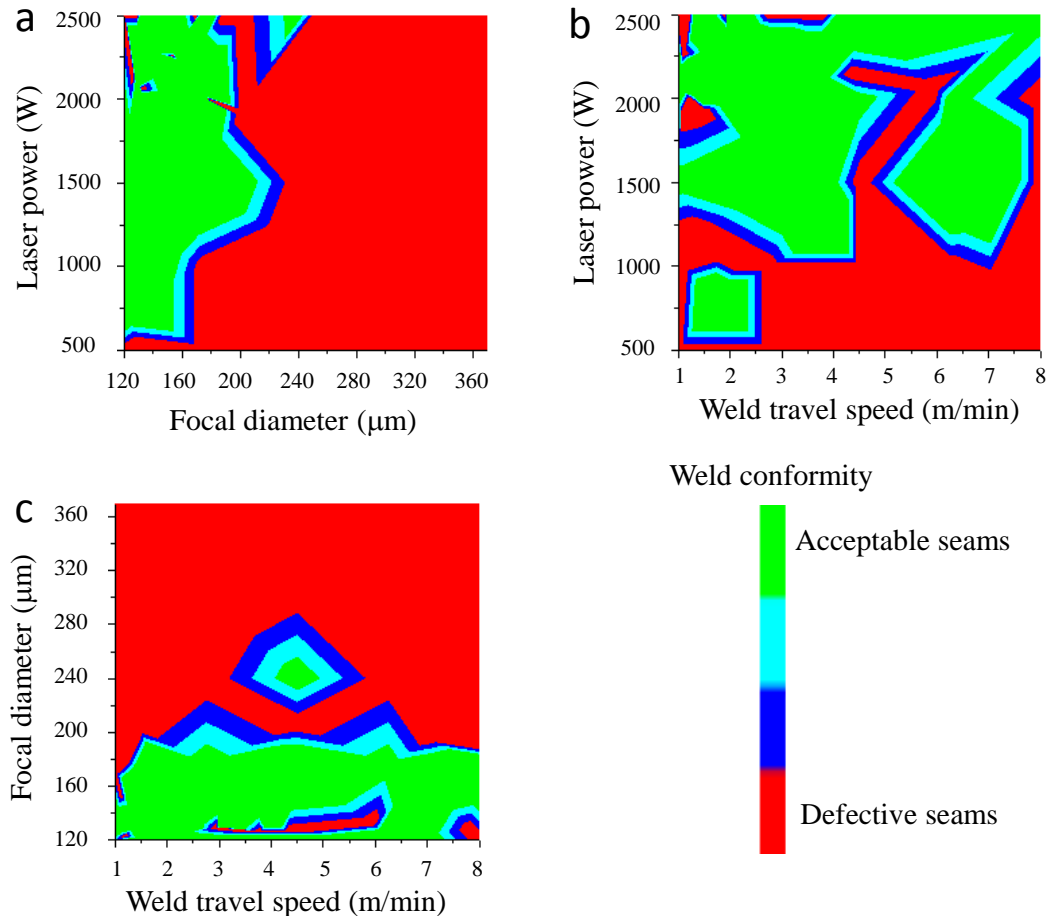
FIGURE 8: Response surfaces showing the effect of weld parameter interaction on weld conformance

Correlation analysis and regression modelling were obtained using CORICO software for each response (Table 4). The regression model was defined to find the model with the smallest standard error. The CORICO model accounts for logical interactions in the equations. The meaning of each logical interaction in the equations presented is as follows:

- X1&X2 means that Y is high when the value of both X1 and X2 are high,

- X1^X2 means that Y is high when the value either or both X1 and X2 are high,

- X1&-X2 means that Y is high when the value of X1 is high and X2 is low,

- X1-X2 means that Y is high when the difference between X1 and X2 is high,

- X1]X2 means that Y correlates with X1 when X2 is high,

- X1#-X2 means that Y is high when X1 did not vary as X2,

- X1{X2 means that Y is high when X1 is at average and X2 is high,

- X1{-X2 means that Y is high when X1 is at average and X2 is low.

TABLE 4
REGRESSION MODELS FOR EACH RESPONSE AS A FUNCTION OF THE LOGICAL INTERACTIONS OF FACTORS.

Regression models	Correlation coefficient (R)
Core fiber	
Compliant weld = 0. 3611 + 2. 015 Power{-Focal diameter - 0. 8425 Focal diameter{Focal diameter + 1. 111 Power]Speed + 0. 8686 Speed}Focal diameter + 0. 6850 Power!Speed	0. 74
Collapse of the weld bead = 0. 3194 - 1. 914 Speed^Speed + 1. 243 Power]Focal diameter+ 1. 338 Focal diameter{Focal diameter- 0. 9791 Focal diameter]Speed	0. 62
Non-Compliant geometry = 0. 8611 - 1. 506 Speed]Speed - 0. 8527 Speed!Focaldiameter+ 0. 8442 Power]Speed	0. 72
Full penetration = 0. 8194 - 2. 069 Focal diameter&-Power + 0. 9730 Power!Focaldiameter+ 0. 7047 Power&-Power - 0. 6033 Speed&-Speed - 0. 5955 Focal diameter{- Power - 0. 3990 Speed#Focal diameter	0. 83

IV.   CONCLUSION

Laser welding of thin sheet is particularly interesting for aero-structures manufacturers. This work, focused on 1mm thick AA 6061 T4 alloy, allowed determining the processing window in autogenous laser welding, by mean of a dense experimental design. Sound weld is obtained with relatively high power densities, between $5 \ 10^6$ and $2 \ 10^7$ W/cm^2 and an interaction time lower than $6 \ 10^{-3}$ s. Within this domain, porosities diameters remain under 15 μm, no cracks are observed, and weld seams cross sections show a standard compliant geometry. Regression models are proposed for determination of weldability window, but also to describe appearance of main defects. Based on this study, further work will be focused mechanical properties and corrosion behavior of these assemblies.

REFERENCES

[1] X. Zhang, Y. Chen, J. Hu, Recent advances in the development of aerospace materials, Progress in Aerospace Sciences. 97 (2018) 22–34. https://doi. org/10. 1016/j. paerosci. 2018. 01. 001.
[2] N. Kashaev, V. Ventzke, G. Çam, Prospects of laser beam welding and friction stir welding processes for aluminum airframe structural applications, Journal of Manufacturing Processes. 36 (2018) 571–600. https://doi. org/10. 1016/j. jmapro. 2018. 10. 005.
[3] M. C. Chatervedi, ed. , Welding and joining of aerospace materials, Woodhead Publishing, Cambridge, UK : Philadelphia, PA, 2012.
[4] A. A. Gialos, V. Zeimpekis, N. D. Alexopoulos, N. Kashaev, S. Riekehr, A. Karanika, Investigating the impact of sustainability in the production of aeronautical subscale components, Journal of Cleaner Production. 176 (2018) 785–799. https://doi. org/10. 1016/j. jclepro. 2017. 12. 151.
[5] A. Giesen, J. Speiser, Fifteen Years of Work on Thin-Disk Lasers: Results and Scaling Laws, IEEE J. Select. Topics Quantum Electron. 13 (2007) 598–609. https://doi. org/10. 1109/JSTQE. 2007. 897180.
[6] G. Verhaeghe, B. Dance, An assessment of the welding performance of high-brightness lasers and a comparison with in-vacuum electron beams, in: International Congress on Applications of Lasers & Electro-Optics, Laser Institute of America, Temecula, California, USA, 2008: p. 710. https://doi. org/10. 2351/1. 5061340.
[7] J. Alexis, J. D. Beguin, P. Cerra, Y. Balcaen, Yb: YAG Laser Welding of Aeronautical Alloys, MSF. 941 (2018) 1099–1104. https://doi. org/10. 4028/www. scientific. net/MSF. 941. 1099.
[8] O. O. Oladimeji, E. Taban, Trend and innovations in laser beam welding of wrought aluminum alloys, Weld World. 60 (2016) 415–457. https://doi. org/10. 1007/s40194-016-0317-9.
[9] B. Hu, I. M. Richardson, Mechanism and possible solution for transverse solidification cracking in laser welding of high strength aluminium alloys, Materials Science and Engineering: A. 429 (2006) 287–294. https://doi. org/10. 1016/j. msea. 2006. 05. 040.
[10] M. Tiryakioğlu, Solubility of hydrogen in liquid aluminium: reanalysis of available data, International Journal of Cast Metals Research. 32 (2019) 315–318. https://doi. org/10. 1080/13640461. 2020. 1718337.
[11] X. Zhang, T. Huang, W. Yang, R. Xiao, Z. Liu, L. Li, Microstructure and mechanical properties of laser beam-welded AA2060 Al-Li alloy, Journal of Materials Processing Technology. 237 (2016) 301–308. https://doi. org/10. 1016/j. jmatprotec. 2016. 06. 021.
[12] D. Rasmussen, Étude sur la fissuration à chaud de l'alliage 6061 lors du soudage par procédé hybride laser-GMAW /, Université du Québec à Chicoutimi, Chicoutimi, 2008. https://doi. org/10. 1522/030043965.
[13] J. C. Ion, Laser beam welding of wrought aluminium alloys, Science and Technology of Welding and Joining. 5 (2000) 265–276. https://doi. org/10. 1179/136217100101538308.
[14] J. Graneix, J. -D. Beguin, J. Alexis, T. Masri, Influence of Yb:YAG Laser Beam Parameters on Haynes 188 Weld Fusion Zone Microstructure and Mechanical Properties, Metall and Materi Trans B. 48 (2017) 2007–2016. https://doi. org/10. 1007/s11663-017-0989-6.
[15] J. Graneix, J. -D. Beguin, F. Pardheillan, J. Alexis, T. Masri, Weldability of the superalloys Haynes 188 and Hastelloy X by Nd:YAG, MATEC Web of Conferences. 14 (2014) 13006. https://doi. org/10. 1051/matecconf/20141413006.
[16] F. Dausinger, R. Fabbro, D. Grevey, G. Peix, P. Peyre, A. B. Vannes, Caractérisation, modélisation et maîtrise des porosités créées lors du soudage laser Nd-YAG d'alliages d'aluminium, (n. d.) 174.

Physics of Equilibrium and Non-equilibrium Deformation Processes in the Nickel Surface Layer

S. V. Korotkevich

RUP Gomelenergo, Gomel, Belarus

Abstract— *Based on the Hamilton's principle, invariants are proposed to describe the processes of formation and evolution of the structure of the metal interface under friction. These invariants can be used, among other things, in the creation, evolution and destruction of nanomaterials.*

Keywords— *nano, submicro, micro, meso and macro levels of deformation, equilibrium and non-equilibrium deformation, invariants.*

I.   INTRODUCTION

The mechanisms of hardening and destruction of the surface layer of metals, as well as the conditions for its self-organization under equilibrium deformation are well studied [1, 2], which cannot be said about the self-organization of processes under non-equilibrium deformation under conditions of phase instability of the crystal lattice [3]. In accordance with nonlinear mechanics and mesomechanics, plastic flow in a loaded solid is a multi-level process and is associated with the loss of shear stability at the nano, micro, meso, and macro-scale levels [4]. The intensity of external influence determines the structure, properties and mechanisms of destruction of surface layers of metals. The physics of processes occurring on the metal surface under multi-cycle, low-amplitude and alternating tribo-loading is described in [5-8]. The mechanisms of formation of elements of the defective structure for each of the structural levels of deformation (nano, micro, meso and macro) of the surface layer of Nickel under multicycle low-amplitude and alternating deformation, where the high density of dislocations and the local orientation gradient of structural elements in the Nickel crystal lattice plays a fundamental role at each of the scale levels of deformation [3]. Using various model representations, namely, extinction contours, local curvature of the Nickel crystal lattice, and dislocation contributions to the hardening mechanisms, a quantitative assessment of the values of internal stresses and parameters of the defective structure of the Nickel surface layer was carried out under conditions of its phase instability, where the value of internal stresses is comparable and exceeds the value of the elastic modulus of Nickel $\approx$ $2 \cdot 10^{11}$ Pa. The literature sources contain limited data on such highly dispersed materials and their physical and chemical properties [4, 5]. It is generally accepted that the formation of nanoobjects occurs under high-energy influence or intense plastic deformation and / or equal-channel angular compression in the top-down direction, when the material is fragmented from macro, meso, micro to nanoscale as a result of external influence at contact pressures in the GPa [5]. Data on the formation of nanostructures at contact pressures of $\approx$ 0.1÷0.2 kPa in the presence of chemically active substances under conditions of non-equilibrium deformation are extremely limited.

The question of determining the mechanisms and dominant factors that determine the physical, chemical and mechanical properties (amorphous, superplasticity, catalytic activity, etc.) of the metal interface under non-equilibrium deformation remains open. Determination of the basic laws in the field of equilibrium and nonequilibrium deformation is an urgent problem in the creation of nanomaterials with unique properties.

The aim of this work is to study the mechanisms of plastic deformation at various structural-scale levels under conditions of phase instability of the surface layer of nickel under tribo-loading and to determine the basic laws describing the kinetics of hardening and destruction of the surface layer of metals.

This work presents the results of electron microscopical investigation of surface layer microstructures resulted from sliding friction according to dislocation structure study using the method of ferromagnetic resonance (FMR). It analyzes the micro structural destruction mechanism of nickel on the basis of complex data.

II.   EXPERIMENTAL EQUIPMENT AND SAMPLES

The dislocation structure change in the nickel near the surface layer under friction loading was studied by the methods of electron microscopy and ferromagnetic resonance. Polycrystalline nickel of 99.99 % purity was investigated. The samples in

the form of thin disks 5 by 0.1 mm were electrically polished and annealed in a vacuum of 0.133 mPa at 973 K. Friction tests were carried out on an AE-5 type machine with precision positioning of the contact surface. Sliding friction was carried out in the pair Ni-Mo in air, using CIATIM-201 lubricant under a load of 82.3 kPa at a linear speed of 0.5 m·s^{-1}. The average volume temperature of the sample did not exceed 40° C. The correct use of load-speed parameters or the correct use of the scale factor, along with the high sensitivity of the ferromagnetic resonance (FMR) method to structural changes in a thin surface layer with a thickness of ≈ 0.1 μm, made it possible to see oscillating kinetics of changes in the dislocation density and wear intensity in the analysis of experimental data, which allowed to correctly interpret the results obtained, which are in good agreement with the results of work [1]. The electron microscopic investigation of nickel was carried out under a EMV-100 AK and Hitachi-H800 microscope by the thin foil method at a "transillumination". The resolution of the Hitachi H-800 is ≈ 0.1 nm. The foil was produced by thinning down the disks electrolytically from the side opposite to the friction surface using a jet blower polishing unit equipped with a sensitive photodiode bridge that allows controlling the segment's transparency at 0.1 μm depth from the friction surface. The technique for preparing nickel samples for transmission electron microscopy is given in [2].

III.   INVESTIGATION RESULTS AND THEIR DISCUSSION

An analysis of the experimental data given in [3, 5–12] allowed the author, on the basis of Hamilton's principle or principle of least action [13], to establish two main fundamental regularities and to propose a third one, formulated in [3, 14].

This is the first pattern. An asymmetric kinetic relationship between the density of dislocations and the intensity of destruction or wear has been determined, namely, an increase in the density of dislocations to a certain critical value causes hardening of the surface layer. The latter determines the decrease in the intensity of destruction. An inversely proportional relationship has been established between the local gradient of the orientation of the boundaries of the structural elements of the crystal lattice or the density of dislocations at each of the structural-scale levels of deformation and the intensity of destruction of the surface layer of nickel. Thus, the dependence of dislocation density on time is unipolar to the kinetics of wear intensity [5], and the expression is fulfilled:

$$\rho \cdot I = const \tag{1}$$

where p is the dislocation density and I is the wear intensity.

This is the second pattern. The rate of increase (K_1) and decrease (K_2) in dislocation density at tribo-loading is determined by the formed structure and disorientation of the internal interface boundaries. The rate of increase in the density of dislocations during hardening of the surface layer of nickel determines the rate of decrease in the density of dislocations and, accordingly, the relaxation of deformation stresses for one and each cycle of change in strength properties. The expression is executed [13]:

$$\frac{K_1}{K_2} = const \tag{2}$$

where K =ΔH/t.

It should be noted that the constant in expression (2) is close to unity. However, with the accumulation of energy by subsurface layers over time, the fragile fracture mechanism can dominate, which leads to an insignificant increase in the relaxation rate of broadening of the ferromagnetic resonance line (K_2).

This is the third pattern. The main condition for the compatibility of deformation at the scale-structural levels: nano, micro, meso and macro is the fulfillment of the law of conservation of angular momentum, namely, the sum of the angular momenta is zero, which ensures the fulfillment of the condition for grain boundary sliding of structural elements during plastic deformation. The law of conservation of angular momentum is fulfilled [3, 14]:

$$\sum_{i=1}^{N} RotJi = 0 \tag{3}$$

where J_i are streams of defects at the i-th structural-scale level.

We use methods of mathematical physics to describe the processes occurring in the surface layer of Nickel at tribo-loading. The dependence ∆H (t) has a nonlinear wave character (fig. 1).
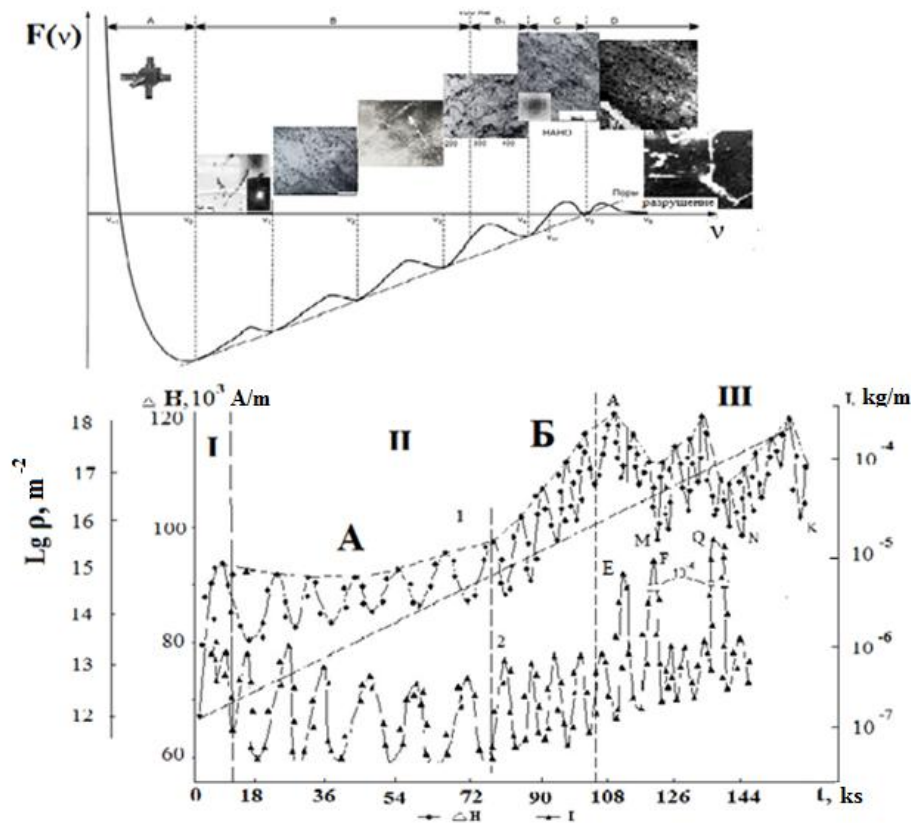
FIGURE 1: Dependence of the kinetics of structural changes in the surface layer of nickel during friction on the Gibbs potential, broadening of the ferromagnetic resonance line (∆H) and wear rate (I).

From the point of view of methods of mathematical physics, if one of the independent variables describing the state of the surface layer of nickel [15] is taken as the broadening of the FMR line (∆H), then the change in the state of the surface layer of nickel under tribo-loading can be described by partial differential equations. We use the wave equation to describe the physics of the processes of deformation and destruction of the nickel surface:

$$\frac{\partial^2 \Delta H}{\partial x^2} = \frac{1}{v^2}\frac{\partial^2 \Delta H}{\partial t^2} \tag{4}$$

Where v – the rate of change in the dislocation density, ∆H – the broadening of the ferromagnetic resonance line.

It is known that the value of the FMR line broadening (∆H) is directly proportional to the dislocation density (p) [5]. We will analyze the wave equation using the experimental data shown in Fig. 1. Consider the region of equilibrium deformation (fig. 1, region II) and the region of non-equilibrium deformation (fig. 1, region III). It should be noted that the ratio of the broadening of the FMR line (∆H) to time (t), defined as the rate of change in the broadening of the FMR line (constant K), is the first derivative ($\frac{\partial \Delta H}{\partial t}$). The second derivative of the broadening of the FMR line with respect to time ($\frac{\partial^2 \Delta H}{\partial t^2}$) is the rate of change ($\frac{\Delta H}{\Delta t}$) of the envelope function ∆H (t) in Fig. 1, which is shown by the dotted line. Let us analyze this envelope for regions II and III in Fig. 1 using the experimentally established boundary conditions.

Equilibrium strain region II consists of two parts: part A and part B (fig. 1). The envelope of the function ∆H (t) for area A can be approximated by a straight line parallel to the axis of time in Fig. 1. Then the expression is executed:

$$\frac{\partial^2 \Delta H}{\partial t^2} = 0. \tag{5}$$

The product of two terms $(1/v^2)$ and $(\frac{\partial^2 H}{\partial x^2})$ in the wave equation (4) is equal to zero and, therefore, the expression is fulfilled:

$$\frac{\partial^2 \Delta H}{\partial x^2} = 0 \cdot \qquad (6)$$

Fick's first law is:

$$J = -\frac{D \cdot dC}{dx} \qquad (7)$$

where J is the diffusion flow of the dislocation density passing through a unit area per unit time, D is the diffusion coefficient, dC/dx is the concentration gradient of the dislocation density in the direction of diffusion. It follows from Fick's first law that the dislocation density flux through a unit area per unit time is a constant value. It is natural to assume that this flow is directed inward from the surface. Considering that the local gradient of the orientation of structural elements (χ) is directly proportional to the dislocation density, it follows that:

$$\frac{\partial \chi}{\partial x} = const \qquad (8)$$

The local gradient of orientation of structural elements (χ) in the direction (OX) is a constant value, which decreases inversely with increasing distance from the surface. Then const must be defined as in the minus of the first degree, and then expression (9) is defined as:

$$\frac{\partial \chi}{\partial x} = const^{-1} \qquad (9)$$

From the analysis of area A of region II in fig. 1, two conclusions follow: the flux of dislocation density through a unit area per unit time is a constant value directed inward from the surface; change in the local gradient of the orientation of structural elements in the direction from the surface is a constant value that decreases in accordance with an inversely proportional relationship with increasing distance from the surface.

Let's go to the analysis of area B of region II in fig. 1. Analysis of the wave equation (4) of area B in fig. 1 shows that the envelope of the rate of change $\Delta H/\Delta t$ is a straight line directed at an angle of 45° to the time axis, since $\frac{\partial^2 \Delta H}{\partial t^2} \approx \frac{120 \kappa A/m - 95 \kappa A/m}{25 \kappa s} \approx 1 A./m \cdot s$. Then the expression is executed:

$$\frac{\partial^2 \Delta H}{\partial t^2} = \frac{1}{v^2}\frac{\partial^2 \Delta H}{\partial x^2} \approx 1 A/m \cdot s \qquad (10)$$

The product of two quantities is equal to one, when each of them is equal to one or minus one. Since the velocity of movement of the dislocation density in the physical sense cannot take a negative value, a system of equations is performed:

$$v = 1 \qquad (11)$$

and

$$\frac{\partial^2 \Delta H}{\partial x^2} = 1 \qquad (12)$$

The velocity of movement of the dislocation density deep from the nickel surface is a constant value, which follows from expression 11. From expression 12, taking into account that, where J is the flow of dislocation density through the unit area per unit time, the expression follows:

$$\frac{\partial J}{\partial x} = 1 \qquad (13)$$

The gradient of dislocation flow deeper from the nickel surface is a constant value. In other words, the number of linear defects (dislocations) passing through a unit of sites built at some distance from each other deep from the surface, per unit of time is a constant value (fig. 2). Quantitative evaluation of expression (13) using shows that for each cycle of change in strength properties in section B of fig. 1, the flow of dislocation density (J) through a unit area per unit time is ≈ 0.25 A / m · s.

Taking into account the fact that the depth of the surface layer of nickel, in which the energy of friction loading is accumulated, is ≈ 100 μkm. Then the depth distribution of the flow (flow gradient) with a step of DX = 25 microns (fig. 2) through the unit area per unit time is ≈ 0.06 A / m · s.
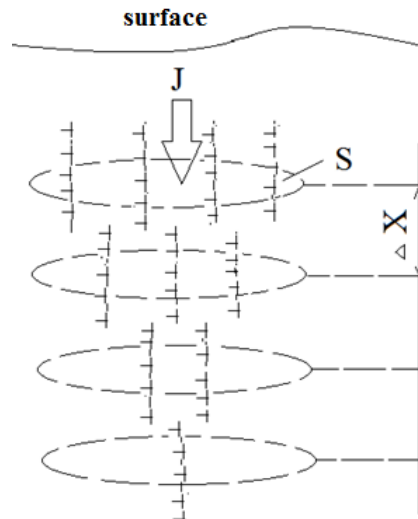
FIGURE 2: Scheme showing a constant gradient of dislocation density flow with increasing distance or depth from the surface

Two conclusions follow from the analysis of area B of region II in Fig. 1: the velocity of movement of the dislocation density deep from the surface is the constant ≈ 1 ((m·s)$^{-1}$); the flow of the dislocation density gradient through a unit of area per unit of time is a constant equal to ≈ 1 (m^{-4}) and is directed deep from the surface.

Analysis of the wave equation (4) in the field of non-equilibrium processes (fig. 1, region III) shows that the envelope of the rate of change ΔH/Δt is an oscillating (periodically increasing and decreasing) dependence over time, that is, the gradient of the dislocation density flow ($\frac{\partial J}{\partial X}$) periodically increases and decreases (fig. 3) and changes its sign, that is, changes its direction.
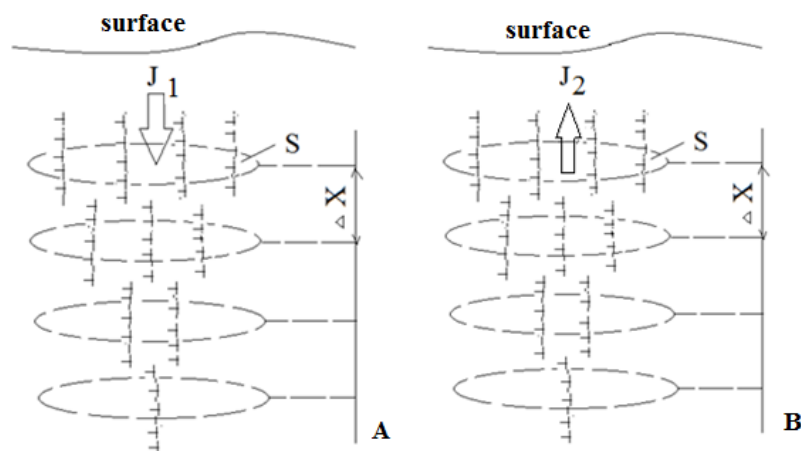
FIGURE 3:Scheme showing a qualitative change in the direction of the flow gradient of the dislocation density with increasing and decreasing changes in the value of stresses inside the nickel crystal lattice with increasing distance or depth from the surface: A-increase in the value of internal stresses; B-decrease in the value of internal stresses.

It should be noted that for area A and B of region II in Fig. 1, only an increase in the absolute value of the envelope was observed, and there was no low-frequency (LF) component (fig. 1, region III). The period of the LF component of the dislocation density flow gradient is 23÷25 ks. The rate of increase of the LF component

$(\dfrac{\partial^2 \Delta H}{\partial t^2} \approx \dfrac{120 \kappa A/m - 95 \kappa A/m}{10 ks} \approx 2,5 A./m \cdot s)$ is designated as K_1',

and the rate of decrease of the LF component

$(\dfrac{\partial^2 \Delta H}{\partial t^2} \approx \dfrac{120 \kappa A/m - 95 \kappa A/m}{6 \kappa s} \approx 4,2 A./m \cdot s)$ is designated as K_2'. The ratio of increase (K_1') to decrease (K_2') of the LF component is ≈ 0.6.

The expression is being executed:

$$\frac{K_1^{'}}{K_2^{'}} = \frac{J_1}{J_2} = 0.6 \tag{14}$$

The gradient of the dislocation density flow (J_2) with a decrease in the stress value exceeds the gradient of the dislocation density flow (J_1) with an increase in the stress value by ≈ 1.7 times. Taking into account the fulfillment of the relation (3), where the sum of defect flows is zero, it follows that to fulfill the condition of plasticity and amorphous surface layers of Nickel within a single cycle of the LF component (not including point M, N and K in fig. 1), the dislocation density flow increases by ≈ 1.7 times when the stress value decreases.

The descending and ascending flows of the defect structure and the oscillating nature of the stresses determine the formation of a highly developed relief (fig. 4), the folds of which can be interpreted as a corrugated surface layer. A high density of dislocations in local zones, in the form of pronounced white dots, determines dynamic recrystallization with the formation of structures with a high modulus of elasticity.
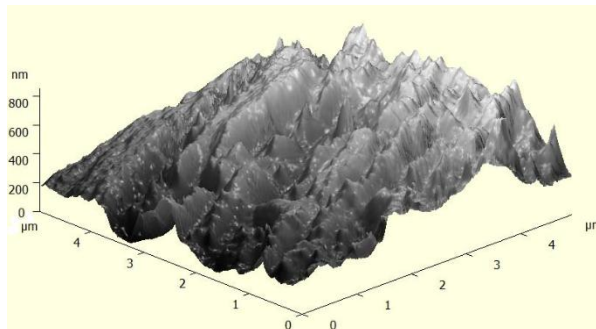
FIGURE 4: Three-dimensional image of the AFM image of the nickel surface with nanostructured formations

At the minimum points (M, N and K) of the dependence of the FMR line broadening (ΔH) on time (t) (fig. 1, curve 1, region III), where an avalanche – like or selective destruction mechanism occurs localized in time with an increase in the wear intensity by two or three orders of magnitude (fig. 1, region III, curve 2, p. F, Q), there is a violation of the law of conservation of momentum, i. e. expression (3).

It implements the principle of least action, where selective destruction mechanism of the porous layer defines the removal of foci of discontinuities of the material (microcracks, pores, twins, defects, etc.) that maintains the durability of the material from the positions of synergetics and prevents the penetration of cracks into the material.

Four conclusions follow from the analysis of area III in Figure 1: the gradient of flow of dislocation density($\dfrac{\partial J}{\partial X}$) periodically increases and decreases on time at tribo-loading; the gradient of flow of dislocation density changes its direction; an increase in the intensity of the gradient of ascending and descending flows of dislocation density causes an increase in the lower limit of the change in the wear intensity by at least ≈ 7 times, and the upper limit of the change in the wear intensity in the avalanche-like selective mechanism of destruction of the surface layer by three orders of magnitude; the gradient of the

flow of dislocation density (J_2) with a decrease in the stress value exceeds the gradient of the dislocation density flow (J_1) with an increase in the stress value by ≈ 1.7 times.

Thus, the amount of accumulation of defects, their size and interaction determine the process of self-regulation in the area of nonequilibrium deformation. The accumulation of defects by the surface layer and the associated increase in the latent deformation energy lowers the activation energy of relaxation processes by so much that these processes, with further deformation, play the role of a kind of regulator of both the number of defects and the way of their interaction and distribution [5].

Analysis of the results obtained using transmission electron microscopy showed [8] that the main microstructural elements of dispersion of the surface layer are: 1) zones with a high density of dislocations, with the time of loading acquiring the form of thin bundles and oriented along the sliding direction; 2) slip bands and numerous thin twins along their boundaries, which are the sources of the initiation of small cracks; 3) numerous micropores inside the deformed lattice and along the grain boundaries, their coagulation leads to the formation of foci of transcrystalline and intercrystalline destruction (fig. 5, A). Prolonged frictional loading leads to progressive loosening of the surface layer of nickel (fig. 5, B), associated with an increase in the number of fracture centers [10]. Nonequilibrium vacancies at nickel lattice sites under plastic distortion form microporosity by the coalescence mechanism, which is a precursor of plastic shear [16 – 18] meso and macroscales that determine the lobe-layer-by-layer mechanism of destruction [12, 19] and avalanche-like selective destruction of the surface [8] into local moment of time.
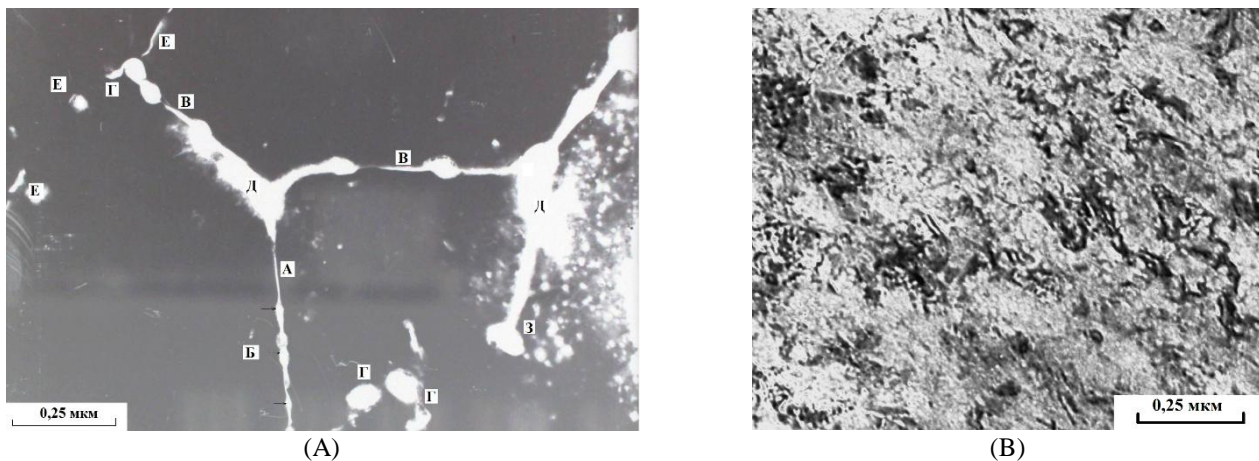
FIGURE 5. A– Pore formation and fracture along grain boundaries and through grain; B – Dispersion and loosening of the surface layer (t = 150 ks)

In a strongly deformed crystal lattice, high porosity develops reaching$\approx 25\%$ of the total volume of the material, and a high concentration of microcracks and other discontinuities in the material [5].

It should be noted that it is necessary to conduct further systemic studies to establish the main invariant regularities.

IV.   CONCLUSION

Analysis of the kinetics of the processes of deformation and destruction of scale levels: nano, submicro, micro, meso and macro using boundary conditions applied to the wave equation shows that:

- In the area of the equilibrium deformation in the absence of a gradient flow structural defects (fig. 1, area A, region II): the flow of the dislocation density is a constant value directed inward from the surface; the change of local gradient of the orientation of structural elements is a constant value that decreases in accordance with an inversely proportional relationship with increasing distance from the surface;

- The intensity of external influence determines the duration of the cycle of changes in strength characteristics, the amount of deformation energy accumulation and the degree of fragmentation of the crystal lattice of metals, and, accordingly, the local gradient of orientation of the boundaries of structural elements, where their geometric size, quantity, density, and interaction determine the dominant role of one or another scale level of plastic deformation at a given time of the kinetics of structure formation, and the mechanism of its destruction in accordance with the

minimum potential energy of interaction of the formed structure in the area of equilibrium deformation in the presence of a flow gradient of structural defects: in the area of equilibrium deformation in the presence of a flow gradient of structural defects: the velocity of the dislocation density movement (fig. 1, area B) deep from the surface is a constant value equal to ≈ 1 (m·s) $^{-1}$; the flow of the dislocation density gradient through a unit of area per unit of time is a constant value of ≈ 1 m^{-4};

- In non-equilibrium deformation ((fig. 1, region III)): the flow gradient of dislocation density changes its direction; the flow gradient of dislocation density ($\frac{\partial J}{\partial X}$) is oscillating in time; an increase in the intensity of the gradient of ascending and descending flows of dislocation density causes an increase in the lower limit of the change in the wear intensity, at least ≈ 7 times, and the upper limit of the change in the intensity of wear by three orders of magnitude at the avalanche selective mechanism of destruction of surface layer; the gradient of the flow of dislocation density (J_2) at decrease in the stress value exceeds the gradient of the dislocation density flow (J_1) at increase in the stress value by $\approx 1. 7$ times.

The principle of least action is implemented, where the selective mechanism of destruction of the porous and amorphous layer determines the removal of foci of discontinuity of the material (microcracks, pores, duplicates, packaging defects, etc.), which determines the preservation of the integrity and continuity of the material.

It has been established that the kinetics of structure formation and evolution of the interface between metals under tribo-loading proceeds in accordance with the following provisions of nonequilibrium thermodynamics:

- Each stable state of the metal interface will have its own structure with a certain value of free energy and, accordingly, with the types of its redistribution between the elements of the boundaries and within the structural formation;

- The system tends to occupy a position or form such a structure of the interface, which corresponds to the minimum thermodynamic Gibbs potential;

- If the action of load-speed parameters or external influence exceeds some critical value of the energy supplied to the system, then it passes into a new structural state characterized by a lower value of free energy;

- The intensity of external influence determines the duration of the cycle of changes in strength characteristics, the amount of deformation energy accumulation and the degree of fragmentation of the crystal lattice of metals, and, accordingly, the local gradient of orientation of the boundaries of structural elements, where their geometric size, quantity, density, and interaction determine the dominant role of one or another scale level of plastic deformation at a given time of the kinetics of structure formation, and the mechanism of its destruction in accordance with the minimum potential energy of interaction of the formed structure.

ACKNOWLEDGEMENTS

REFERENCES

[1] B. Moser, T. Hanlon, K. S. Kumar, "Cyclic Strain Hardening of Nanocryslline Nickel", Scri. Mater, 2006, Vol. 54, No 6, pp. 1151 – 1155.

[2] V. E. Panin [and others],"Surface Layers and Internal Boundaries in Heterogeneous Materials", Novosibirsk: SO RAN, 2006, 520 p.

[3] V. E. Panin, V. G. Pinchuk, S. V. Korotkevich, S. V. Panin,"Multiscaling of Lattice Curvature on Friction Surfaces of Metallic Materials as a Basic of Their Wear" *Mechanism Physical Mesomechanics*, Vol. 20, No 1, 2017, pp. 69 – 77.

[4] V. E. Panin, V. E. Egorushkin, A. V. Panin, "Physical Mesomechanics of a Deformable Solid as a Ultilevel System. I. Physical Foundations of a Multilevel Approach", *Physical Mesomechanics*, 2006,Vol. 9, No 3, pp. 9–22.

[5] V. G. Pinchuk, S. V. Korotkevich,"Kinetics of Hardening and Destruction of Metal Surface During Friction", LAP Lambert Academic Publishing, Saarbrŭcken: LAP, 2014, 180 p.

[6] S. V. Korotkevich, V. G. Pinchuk, V. V. Kravchenko,"Diagnostics of Rolling and Sliding Bearings by the State of the Interface of Conjugate Bodies by Physical Methods" LAP Lambert Academic Publishing, Saarbrŭcken: LAP, 2016, 266 p.

[7] V. G. Pinchuk, S. V. Korotkevich,"Physical Patterns of Dislocation Structure Kinetics in Friction Loaded Surface Layers",*Global Journal for Research Analysis*, No4, issue No 5, 2015, pp. 255–257.

[8] V. G. Pinchuk, I. A. Buyanovskiy, S. V. Korotkevich, "Kinetics of Microstructure and Selective Mechanism of Fracture of Metal Surface Layer under Friction", *Inorganic Materials: Applied Research*, 2015, Vol. 6, No 5,pp. 355–359.

[9] V. G. Pinchuk, S. V. Korotkevich, "Microstructure Evolutionin Friction- Loaded Layers of Nickel" *Indian Journal of Research*, Vol. No 4, issue№ 2, 2015, pp. 8–10.

[10] V. G. Pinchuk, S. V. Korotkevich, E. A. Kovalev, "Relationship of Microstructural Criteria of Fracture and Evolution of Metal Surface and Physicochemical Properties of Medium at Friction",*Inorganic Materials: Applied Research*, 2017, Vol. 8, No 4,pp. 539–545.

[11] V. G. Pinchuk, S. V. Korotkevich, E. A. Kovalev, "Influence of the Physical and Chemical Nature of Quenching Medium and Friction Regimes on the Structure and Kinetics of Hardening and Destruction of the Surface Layer of Nickel", *Inorganic Materials: Applied Research*, 2018, Vol. 9, No 4, pp. 736 –740.

[12] S. V. Korotkevich, V. V. Sviridova, "Structural-Scale Levels of Deformation of the Surface Layer of Nickel", *Problems of Physics, Mathematics and Technology*, 2020, No. 2,pp. 17–22.

[13] S. V. Korotkevich, "Hamilton's Principle for to Search of Invariants at Creation, Evolution and Destruction of Nanomaterials"**,** *International Journal of Engineering Research and Science*, 2018, Vol. 4, issue 6, pp. 31–41.

[14] V. E. Panin, "Physical Foundations of Mesomechanics of a Medium with Structure",*Izv. Universities. Physics*, 1992,Vol. 35, No 4, pp. 5–18.

[15] G. Nicolis, N. Prigozhin, "Self-Organization in Non-Equilibrium Processes, M. : Mir, 1977, 512 p.

[16] I. Intrater, E. S. Machlin,"Grain Boundary and Intercristalline Cracking, *Acta Metal*, 1959, V. 7, No 2, pp. 140 – 142.

[17] P. Neuman, "Coarse Slip Model of Fatigue",*Acta metallurgical*, 1969, Vol. 17, No9. – pp. 1219–1225.

[18] C. Holste,"Cyclic Plasticity of Nickel, from Single Crystals to Submicrocrystalline Polycrystals", *Philosophical Magazine*, 2004, Vol. 84, No 3–5, – pp. 299–315.

[19] N. P. Suh, "An Overview of the Delamination Theory of Wear", *Wear*, 1977, Vol. 44, No 1, pp. 1 – 16.

Antioxidant activity and Phytochemical Evaluation of *Piper species* (*Cubeba and Nigrum*)

Angad Verma[1*], Sangamesh B. Puranik[2], Rohit Saraswat[3], Ritu Sharma[4], Prashant Sharma[5]

School of Pharmacy, OPJS University, Churu, Rajasthan

Abstract— *Indian spices that provide flavor, color, and aroma to food also possess many therapeutic properties. Ancient Indian texts of Ayurveda, an Indian system of medicine, detailed the medicinal properties of these plants and their therapeutic usage. Recent scientific research has established the presence of many active compounds in these spices that are known to possess specific pharmacological properties. The therapeutic efficacy of these individual spices for specific pharmacological actions has also been established by experimental and clinical studies. The medicinal effects traditionally ascribed to Indian spices are validated by modern pharmacological and experimental techniques, thus providing a scientific rationale to their traditional therapeutic usage. Many plant-derived molecules have shown a promising effect in therapeutics. Among the plants investigated to date, one showing enormous potential is the Piperaceae. Piperine is an alkaloid found naturally in plants belonging to the pyridine group of Piperaceae family, such as Piper nigrum and Piper cubeba. It is widely used in various herbal cough syrups and it is also used in anti inflammatory, anti malarial, anti leukemia treatment. So the present study was aimed to extract the phytochemical compounds in different solvent system in Piper nigrum and Piper cubeba. In preliminary screening and confirmatory test it was identified as alkaloid. High antioxidant activity was found in Piper cubeba ethanol extract i.e. 77.61±0.02% in comparison to Piper nigrum extracts with 74.61±0.02% with IC_{50} values 10.54±0.12μg/mg and 14.15±0.02 μg/mg respectively.*

Keywords— *Piper nigrum, Piper cubeba, Phytochemical, Antioxidant activity, DPPH.*

I.   INTRODUCTION

Many plant derived molecule have shown a promising effect in therapeutics (Lokhande *et al*., 2007). Spices and herbs are recognized as sources of natural antioxidants and thus play an important role in the chemoprevention of diseases and aging. Among the plants investigated to date, one showing enormous potential is the pepper family otherwise known as Piperaceae (Dodson *et al*., 2000). *Piper nigrum* and *Piper cubeba* are the two flowering vine in the family Piperaceae. *Piper nigrum* (black pepper) it is a monocious or decorous climbing vine native to southern India and Srilanka and is extensively cultivated there and elsewhere in tropical regions. The shout climbing stem are very flexible with leathery blackish green leaves, they are widely cultivated in tropics. They have several uses such as they help in pain relief, rheumatism, chills, flu, colds, muscular aches and fever. Externally it is used for its rubefacient and as a local application for relaxed sore, throat and some skin disorder. It has antimicrobial (Dorman and Deans, 2000), antimutagenic (El-Hamss *et al*., 2003), antioxidant and radical scavenging property (Gulcin, 2005) and inhalation of black pepper oil increase the reflexive swallowing movement cultivated for its fruit and essential oil. It is mostly grown in Java and Sumatra, hence sometimes called Java pepper. This is a perennial plant, with a climbing stem, round branches, about as thick as a goose-quill, ash-colored and rooting at the joints. The leaves are from four to six and a half inches long by one and a half to two inches broad, ovate-oblong, acuminate and very smooth. Flowers arranged in spikes at the end of the branches; fruit, a berry rather longer than that of black pepper. It is used to treat gonorrhea, dysentery, syphilis, abdominal pain and asthma (Eisai, 1995) and has also inhibitory effect on hepatitis C virus protease. Choi and Hwang (2003) demonstrated anti inflammatory and analgesic activity of methanol extract from the fruit of *Piper cubeba* it accumulates lignans and essential oil in a relatively high amount.

The alkaloids, of which some 5,500 are known, comprise the largest single class of secondary plant substance. Alkaloids are often toxic to man and many have dramatic physiological activities; hence their wide use in medicine. They are usually colorless, often optically active substances, most are crystalline but a few (e.g. nicotine) are liquids at room temperature. Piperine is an alkaloid found naturally in plants belonging to the pyridine group of Piperaceae family, such as *Piper nigrum* and *Piper longum*. Piperine is the Trans stereoisomer of 1-piperoylpiperidine. It is also known as (E, E)-1- piperoylpiperidine and (E, E)-1- [5-(1, 3- benzodioxol-5-yl)-1-oxo-2, 4-pentdienyl] piperidine. Piperine is the alkaloid responsible for the pungency of black pepper and long pepper, along with chavicine (an isomer of piperine). It has also been used in some forms of traditional medicine and as an insecticide. Majeed (1999) reported that piperine is widely used in various herbal cough

syrups for its potent anti-tussive and bronchodilator properties. It is used in anti inflammatory, anti malarial, anti leukemia treatment. Recent medical studies have shown that it is helpful in increasing the absorption of certain vitamins, selenium, β-cartene, also increase the body's natural thermogenic activity.

The dried cubeb berries contain essential oil consisting monoterpenes (sabinene 50%, α-thujene, and carene) and sesquiterpenes (caryophyllene, copaene, α- and β-cubebene, δ- cadinene, germacrene), the oxides 1,4- and 1,8-cineole and the alcohol cubebol. About 15% of a volatile oil is obtained by distilling cubebs with water. Cubebene, the liquid portion, has the formula $C_{15}H_{24}$. It is a pale green or blue-yellow viscous liquid with a warm woody, slightly camphoraceous odor (Lawless and Julia, 1995). After rectification with water, or on keeping, this deposits rhombic crystals of camphor of cubebs. In India, Sanskrit texts included cubeb in various remedies. Charaka and Sushruta prescribed a cubeb paste as a mouthwash, and the use of dried cubebs internally for oral and dental diseases, loss of voice, halitosis, fevers, and cough. Unani physicians use a paste of the cubeb berries externally on male and female genitals to intensify sexual pleasure during coitus. Due to this attributed property, cubeb was called "Habb-ul-Uruus" (Khare, 2004). In traditional Chinese medicine cubeb is used for its alleged warming property. In Tibetan medicine, cubeb (ka ko la in Tibetan) is one of bzang po drug, six fine herbs beneficial to specific organs in the body, with cubeb assigned to the spleen (Stearns and Cyrus, 2000). Arab physicians of the Middle Ages were usually versed in alchemy, and cubeb was used, under the name Kababa, when preparing the water of al butm (Patai and Raphael, 1995).

In the present study an attempt was made to screen different multi solvent extracts prepared from dried fruits of *Piper nigrum* and *Piper cubeba* to study the antioxidant activity on basis of their phytochemical significance.

II. MATERIALS AND METHODS

2.1 Plant material

The dry fruits of *Piper nigrum* and *Piper cubeba* were collected from local tribal people of Koraput, Mayurbhanj District, Odisha. Then they were washed thoroughly in distilled water and the surface water was removed by air drying under shade. The leaves were subsequently dried in a hot air oven at 40 ^{0}C for 48h, powdered and used for extraction.

2.2 Preparation of crude extract

50gms of dry powdered fruits of *Piper nigrum* and *Piper cubeba* were extracted successively with double distilled water, ethanol and methanol (each 400ml.) for 10-12 hrs. through Soxhlet apparatus method. Then collected solutions were filtered through Whatman No-1 filer paper. The extracts were evaporated to dryness under reduced pressure at 90^{0}C by Rotary vacuum evaporator to obtain the respective extracts and stored in a freeze condition at −18^{0}C until used for further analysis.

2.3 Qualitative screenings of phytochemicals

The qualitative screenings of powdered crude drugs for their active ingredients were carried out using the following standard procedures (Trease and Evans, 1983; Indian Pharmacopeias, 1996; Mukherjee, 2002; Horborne, 2005).

2.4 Phenolic estimation

The total phenol content of plant extracts were determined by using Folin-Ciocalteu Spectrophotometric method according to the method described (Kim *et al*., 2007). Reading samples on a UV-vis spectrophotometer at 650 nm. Results were expressed as Catechol equivalents (μg/mg).

2.5 Antioxidative activity

The evaluation of radical scavenging activity (antioxidant activity) was conducted by the method of (Blois, 1958) with modifications. The following concentrations of extracts were prepared 40μg/mL, 80μg/mL, 120μg/mL, 160μg/mL and 200μg/mL. A stock solution of the sample (100mg/ml) was diluted for 5 concentrations. Each concentration was tested in triplicate. The portion of sample solution (0.5ml) was mixed with 3.0ml of 0.1mM 1,1-Diphenyl-2-2picrylhydrazyl (DPPH, in 95% distilled ethanol) and allowed to stand at room temperature for 30 minute under light protection. The absorbance was measured at 517nm.The scavenging activity of the samples at corresponded intensity of quenching DPPH. Lower the absorbance of the reaction mixture indicates higher free radical scavenging activity. The different in absorbance between the test and the control (DPPH in ethanol) was calculated and expressed as (%) scavenging of DPPH radical. The capability to scavenge the DPPH radical was calculated by using the following equation.

$$\text{Scavenging effect } (\%) = (1 - \frac{A_s}{A_c}) \times 100 \hspace{4cm} (1)$$

As is the absorbance of the sample at t =0 min.

Ac is the absorbance of the control at t=30 min

In the DPPH test, antioxidants were typically characterized by their IC_{50} value (Inhibition Concentration of Sample required to scavenge 50% of DPPH radicals). The results were obtained by linear regression analysis of the dose response curve plotted using % inhibition and concentration.

III.   RESULTS AND DISCUSSION

3.1   Phytochemical screening

In the present study, preliminary phytochemical testing shows (Table-1), the presence of high amount of glycosides, alkaloids, tannins, phenolics and other all the principal secondary metabolites were detected in ethanolic extract of *Piper nigrum* and *Piper cubeba.* The living system is protected from this by enzymes such as superoxide dismutase, glutathione peroxidase and catalase and certain endogenous antioxidant such as α–tocopherol, ascorbic acid, β–carotene and uric acid, since the endogenous antioxidants acting as intracellular defense systems protecting cells from free radicals damage and extensive lyses (Sies and Stahl., 1995; Pietta, 2000). Scavenging and diminishing the formation of oxygen-derived species are not 100% efficient, micro nutrients or antioxidants taken as supplements are particularly important in diminishing the cumulative oxidative damages (Vani *et al.*, 1997).

Atal *et al.*, (1985) showed that biochemical basis enhanced drug availability by piperine. The phytochemical screening and quantitative estimation of the percentage crude yields of chemical constituents of the plants studied showed that the leaves and stems were rich in alkaloids, flavonoids, tannins and saponins. They were known to show medicinal activity as well as exhibiting physiological activity (Sofowara, 1993). Steroids and phlobatannins were found to be present in all the plants. It has been found that some of these investigated plants contained steroidal compounds.

TABLE 1
PRELIMINARY PHYTOCHEMICAL SCREENING OF PIPER NIGRUM AND *PIPER CUBEBA*

Plant's Name	Alkaloid	Glycosides	Terpenoid	Steroid	Flavonoid	Tannins	Reducing Suger	Anthra-quinones
Piper nigrum	+	+	+	+	+	+	+	+
Piper cubeba	+	+	-	+	+	+	-	+

(+) Denotes average and (--) denotes absent

3.2   The effect of different solvents on the yields of crude extracts

The significant variation in the yields of *Piper nigrum* and *Piper cubeba* extracts were shown using various fraction solvents.

The yield of extracts using Water, Methanol and Ethanol in case of *Piper nigrum* were 2.80gm, 2.45gm and 3.35gm respectively. Likewise the *Piper cubeba* extract also followed the same order as the *Piper nigrum* extracts, and they were 1.51gm, 1.75gm and 2.56gm. The variation in yield may be due to the polarity of the solvents used in the extraction process (Table-3).

3.3   Total phenolic content

Medicinal plants are an important source of antioxidants (Rice-Evans, 2007). Natural anti-oxidants increase the anti-oxidant capacity of the plasma and reduce the risk of certain diseases (Prior and Cao, 2000). Polyphenols are the major plant compounds with anti-oxidant activity. Typical phenolics that possess anti-oxidant activity are known to be mainly phenolic acids and flavonoids (Demiray *et al.*, 2009). It is reported that the phenolics are responsible for the variation in the anti-oxidant activity of the plant (Luo *et al.*, 2004). They exhibit anti-oxidant activity by inactivating lipid free radicals or preventing decomposition of hydro peroxides into free radicals (Pokorny 2001; Pitchaon *et al.*, 2007). *Piper cubeba* showed the highest Phenolic content i.e. 123.1±0.05(µg/g) in comparison to *Piper nigrum* with 62.3±0.08(µg/g) (Table-2).

TABLE 2

PHENOL CONTENT OF PIPER CUBEBA AND PIPER NIGRUM FRUITS IN ETHANOLIC EXTRACTS.

Solvent	Total phenols (µg/g)	
	Piper cubeba	*Piper nigrum*
Ethanol	123.1±0.05	62.3±0.08

TABLE 3

CRUDE EXTRACTS AND IC$_{50}$ VALUES PIPER NIGRUM AND PIPER CUBEBA IN DIFFERENT SOLVENT EXTRACTS

Solvent used	*Piper cubeba*		*Piper nigrum*	
	Crude Extracts (gm)	IC50 Value (µg/ml)	Crude Extracts	IC50 Value (µg/ml)
Water	4.30	-------	3.51	-------
Methanol	4.15	-------	3.75	-------
Ethanol	4.35	10.54±0.12	3.56	14.15±0.02

3.4 DPPH free radical scavenging activity

The stable radical DPPH has been used widely for the determination of primary anti-oxidant activity (Brand-Williams *et al*., 1995; Katalinic *et al*., 2004). DPPH stable free radical method is an easy, rapid and sensitive way to survey the antioxidant activity of a specific compound or plant extracts (Koleva *et al*. 2002). It is accepted that the DPPH free radical scavenging by antioxidants is due to their hydrogen donating ability (Chen *et al*. 1995). The collected fruit extracts exhibited remarkable DPPH free radicals scavenging ability at different concentrations. From these, the % inhibition concentrations and IC$_{50}$'s were calculated.

TABLE 4

DPPH SCAVENGING ACTIVITY PIPER CUBEBA AND PIPER NIGRUM IN DIFFERENT SOLVENT EXTRACTS

Conc. of extracts (µg/ml)	Antioxidant activity (%)					
	Water		Methanol		Ethanol	
	Piper cubeba	*Piper nigrum*	*Piper cubeba*	*Piper nigrum*	*Piper cubeba*	*Piper nigrum*
50	35.38±0.02	28.15±0.01	58.07±0.04	53.07±0.04	68.69±0.04	61.69±0.04
100	37.69±0.08	31.00±0.03	60.92±0.06	56.92±0.06	70.23±0.05	62.23±0.05
150	40.00±0.10	34.30±0.04	63.00±0.09	60.00±0.09	72.76±0.04	66.76±0.04
200	42.30±0.07	36.61±0.03	67.53±0.07	61.53±0.07	74.30±0.03	69.30±0.03
250	45.84±0.05	39.92±0.02	69.84±0.05	63.84±0.05	77.61±0.02	74.61±0.02

Table-4 shows the results of the free radical (DPPH) scavenging activity in % inhibition. The result revealed that the ethanol fraction of *Piper cubeba* exhibited the highest radical scavenging activity with 77.61±0.02 followed by its methanolic extract with 69.84±0.05and aqueous extract with 45.84±0.05. In comparison to *Piper cubeba* and *Piper nigrum* extract shows less scavenging activity. The *Piper nigrum* extract of obtained from ethanol shows 74.61±0.02 i.e. highest scavenging activity followed by its methanolic extract with 63.84±0.05and aqueous extract with 39.92±0.02. In overall comparison the ethanolic extract of both *Piper cubeba* and *Piper nigrum* seeds show the highest scavenging activity followed by the aqueous and then methanol. Methanol and ethanol has been proven as effective solvent to extract phenolic compounds. Among solvents used in this study ethanol has showed the best effectiveness extracting phenolic components. Ethanol is preferred for the extraction of antioxidant compounds mainly because its lowers toxicity Karadeniz *et al*., (2005). The antioxidant activities of the individual compounds may depend on structural factors, such as the number of phenolic hydroxyl or methoxyl groups, flavone hydroxyl, keto groups, free carboxylic groups and other structural features (Patt *et al*., 1990). Piper species, commonly used in diet and traditional medicine, were assessed for their antioxidant potential. Catalase activity predominated in *Piper longum* Linn., followed by *Piper cubeba* Linn., green pepper, *Piper brachystachyum* Linn. and *Piper nigrum* Linn. Black pepper (*Piper nigrum* Linn.) was richest in glutathione peroxidase and glucose-6-phosphate dehydrogenase, green pepper was richest in peroxidase and vitamin C, while vitamin E was greater in *Piper longum* Linn. and *Piper nigrum* Linn.

Piper brachystachyum Linn. and *Piper longum* Linn. were rich sources of vitamin A (Aqil *et al*., 2006). The antioxidant and radical scavenging activities of black pepper (*Piper nigrum* Linn.) seeds have been well reported (Gulcin, 2005). Both water extract and ethanol extract of black pepper exhibited strong antioxidant activity. Antioxidant, superoxide, dismutase, and catalase activities of *Piper cubeba* Linn have been reported (Aqil *et al*., 2006; Karthikeyan and Rani, 2003; Choi and Hwang, 2005).

3.5   IC$_{50}$ value

IC$_{50}$ value is defined as the concentration of substrate that causes 50% loss of the DPPH activity and was calculated by linear regression mentioned of plots of the percentage of antiradical activity against the concentration of the tested compounds. Results showed in Table-3 reports no IC$_{50}$ value in water and methanol extraction of both the plants. Only ethanolic extract of the two plants showed an IC$_{50}$ value of 27.34µg/mg in case of *Piper nigrum* and 14.51µg/mg in case of *Piper cubeba*. The ethanolic extract of *Piper nigrum* exhibited significant activity with low IC$_{50}$ value in comparison to *Piper cubeba*. The antioxidant activity of *Piper nigrum* and *Piper cubeba* extracts rise with the rising of polyphenol content of the extract. Similar results were obtained by Nooman *et al*., 2008, in which the crude methanolic extracts of *Piper cubeba* Linn. and *Piper nigrum* Linn. showed antioxidant activity, with IC$_{50}$ values 11.3 ± 0.3µg/ml and 144.1 ± 2.2µg/ml respectively. A linear relationship between the reciprocal of IC$_{50}$ value and the total polyphenol content of *Piper nigrum* and *Piper cubeba* was observed in this study, indicating that increasing the polyphenol content strengths the antioxidant activity. This finding is similar to that reported by Katsube *et al*. (2004).

IV.   CONCLUSION

The phytochemical tests indicated the presence of alkaloids, glycosides, tannins, and flavonoids in the crude ethanolic extract. Several of such compounds are known to possess potent antioxidant activity. Some of these constituents have already been isolated from this plant. The results of antioxidant activity indicate higher free radical scavenging activity in ethanolic extracts of *Piper cubeba* in comparison to *Piper nigrum* due to presence of phytochemical constituents especially polyphenols. This experiment supports that these fruits can be used in pharmaceutical industries as natural antioxidants.

ACKNOWLEDGEMENTS

REFERENCES

[1]   Atal C.K., Dubey A.K., Singh J. Biochemical basis of enhanced drug availability by piperine, J. Exp. Ther. 1985; (232): 258-262.

[2]   Aqil F., Ahmed I., Mehmood Z. Antioxidant and free radical scavenging properties of twelve traditionally used Indian medicinal plants. Turk J Biol. 2006;(30): 177-183.

[3]   Blois, M.S. Antioxidant determinations by the use of a stable free radical. Nature. 1958; 181: 1199-1200.

[4]   Brand-Williams W., Cuvelier M.E. and Berset C. Use of free radical method to evaluate antioxidant activity. Lebensmittel Wissenschaft and Technologie. 1995; 28(1):25-30.

[5]   Choi E.M., Hwang J.K. Effect of some medicinal plants on plasma antioxidant system and lipid levels in rats. Phytother Res. 2005;(19):382-386.

[6]   Demiray S., Pintado M.E. and Castro P.M.L. Evaluation of phenolic profiles and antioxidant activities of Turkish medicinal plants: Tilia argentea, Crataegi folium leaves and Polygonum bistorta roots. World Acad. Sci. Eng. Technol.,2009;(54):312-317

[7]   Dodson C.D., Dyer L.A., Searcy J., Wright Z., Letourneau D.K. Cenocladamide, a diydropyridone alkaloid from Piper cenocladum. Phytochemistry. 2000;(53): 51-54.

[8]   Dorman H.J., Deans S.G. Antimicrobial agents from plants: antibacterial activity of plant volatile oils. J Appl Microbiol. 2000;(88):308-316.

[9]   HR E.l., Idaomar M., Alonso-Moraga A., Muñoz S.A. Antimutagenic properties of bell and black pepper. Food Chem. Toxicol. 2003;41(1):41-47.

[10] Eisai P.T. Medicinal Herb Index in Indonesia. 2nd edition. Dian Rakyat, Jakarta. (1995) 21.

[11] Gulcin I. The antioxidant and radical scavenging activities of black pepper seeds. Int J Food Sci Nutr. 2005(56):491-499,

[12] Harborne J.B. Phytochemical Methods, a guide to modern techniques of plant analysis, 3rd Edn. Springer (India) Private Limited, New Delhi (1998).

[13] Indian Pharmacopoeia, Government of India, Ministry of Health & Family Welfare, The controller of publications, Delhi, 1996. VoL. I & II.

[14] Karadeniz F., Burdurulu H.S., Koca N., Soyer Y. Antioxidant activity of selected fruits and vegetables grown in Turkey. Journal of Agriculture and Food Chemistry 2005;(29):297-303.

[15] Karthikeyan J., Rani P. Enzymatic and non-enzymatic antioxidants in selected Piper species. Indian J Exp Biol 2003;(41):135- 140,

[16] Katalinic V., Milos M., Modun D., Music I., Boban M. Antioxidant effectiveness of selected wines in comparison with (+)- calectin. Food Chemistry. 2004;(86):593-600.

[17] Katsube T., Tabata H., Ohta Y., Yamasaki Y., Anuurad E., Shiwaku K., YamaneY. Screening for antioxidant activity in edible plant products: Comparison of low density lipoprotein oxidation assay. Journal of Agriculture and Food Chemistry. 2004;52(8):2391-2396.

[18] Khare C.P. Indian herbal remedies: rational western therapy, Ayurvedic and other traditional usage, Botany, Springer. (2004).

[19] Kim K.T., Yoo K.M., Lee J.W., Eom S.H., Hwang I.K., Lee

[20] C.Y. Protective effect of steamed American ginseng (Panax quinquefolius L.) on V79-4 cells induced by oxidative stress. J. Ethnopharm. 2007;(111):443-445.

[21] Koleva I.I.,. Van Beek T.A, Linssen J.P.H., de Groot A. and. Evstatieva L.N. Screening of plant extracts for antioxidant activity: A comparative study on three testing methods. Phytochem. Anal. 2002;(13): 8-17.

[22] Lawless and Julia. The illustrated encyclopedia of essential oils: the complete guide to the use of oils in aromatherapy and herbalism, Element Books. (1995).

[23] Lokhande P.D., Gawai K.R., Kodam K.M., Kuchekar B.S. Antibacterial activity of extract of Piper longum, J. Pharmacol. Toxicol. 2007;2(6): 574- 579.

[24] Luo Q., Cai Y., Sun M., Corke H. Antioxidant activity and phenolic compounds of 112 traditional Chinese medicinal plants associated with anticancer. Life Science. 2004;(74):2157-2184.

[25] Majeed M., Badmeev V., Rajendran R. Use of piperine as a bioavailability enhancer. United States Patent. 1999;(5):972,382.

[26] Mukherjee P.K.. Quality Control of Herbal Drugs, an approach to evaluation of botanicals, 1st Edn. Business Horizons, New Delhi, 2002.

[27] Nooman Khalaf A., Shakya Ashok K., Al-OZthman Atif, Zaha, El-agbar Farah Husni. Antioxidant Activity of Some Common Plants. Turk J Biol. 2008; 32:51-55.

[28] Patt D. E. and Hudson B. J. F. Natural antioxidants not exploited commercially. In: food antioxidants. Hudson B. J. F., Ed: Elsevior Applied Science: London, U. K. (1990) 171-191.

[29] Pietta P.G. Flavonoids as antioxidants. J Nat Prod. 2000; (63):1035-42.

[30] Pitchaon M., Suttajit M., Pongsawatmani R. Assessment of phenolic content and free radical scavenging capacity of some Thai indigenous plants. Food Chem. 2007; (100):1409-1418.

[31] Pokorny J., Yanishlieva N., Gordon M. Antioxidants in food, Practical Applications,Cambridge Woodhead publishing limited 2001;72(5):145-71.

[32] Rice-Evans C.A., Miller N.J. and Paganga G. Antioxidant properties of phenolic compounds. Trend. Plant Sci. 1997;2:152-159.

[33] Sies H., Stahl W. Vitamin E and C, beta carotene and other carotenoids as antioxidants. Am J Clin Nutr. 1995; 62:13115S-21S.

[34] Sofowara A. Medicinal plants and Traditional medicine in Africa. Spectrum Books Ltd, Ibadan, Nigeria. (1993) 289.

[35] Stearns and Cyrus. Hermit of go cliffs-timeless instructions of a Tibetan mystic, wisdom publication, 2000. ISBN 0-86171-164-5.

[36] Trease G.E., Evans W.C. Pharmacognosy, 12th edn. Bailliere Tindall, East Bourne, 1983. BN213UN.

[37] Vani T., Rajani M., Sarkar S. and Shishoo C. J. Antioxidant properties of the Ayurvedic formulation Triphala and its constituents. Int. J. Pharmacognosy. 1997;35(5): 313–317.

[38] Vijayakumar R.S., Surya D., Nalini N. Antioxidant efficiency of black pepper and piperine in rats with high fat diet induced oxidative stress. Redox Rep. 2004;9(2):105-110.

Design Development and Evaluation of Acyclovir Loaded Compressed Microsponge

Kranti Kumar Bajpai[1*], Sangamesh B. Puranik[2], Rohit Saraswat[3], Ritu Sharma[4], Prashant Sharma[5]

School of Pharmacy, OPJS University, Churu, Rajasthan, India

***Abstract*—** *The Microsponge Drug Delivery System (MDS) is a patented technology has been successively used for the controlled release of topical agents which consist of macro porous beads, typically 10-25 microns in a diameter, which are loaded with active agent. Allowing a sustained flow of substances out of the sphere, the outer surface is typically porous, This system can suspend or entrap a wide variety of substances, and incorporated into a formulated product such as a liquid, gel, cream, or powder. The Microsponge shows time mode release when applied to the skin and they also response to other stimuli like rubbing, pH, etc. MDS technology is currently used in different dosage forms like cosmetics, over the counter (OTC) skin care, sunscreens and prescription products. Microsponge technology allows entrapment of ingredients and it also shows reduced side effects, more stability, increased elegance and enhanced formulation flexibility. In addition, various studies have showed that microsponge systems are non-irritating, non-mutagenic, non-allergenic, and non-toxic. Microspheres can be prepared by different methods using emulsion system or by suspension polymerization in liquid system.*

Keywords*— *Microsponge, Porous-beads, controlled-release, Quisi-emulsion-solvent- diffusion method, Liquid-liquid-suspension-method.

I. INTRODUCTION

1.1 The Microsponge Delivery System

A Microsponge drug delivery system (MDDS) is a patented, highly cross-linked, porous, polymeric microspheres polymeric system (10-25 μ) consisting of porous microspheres particles consisting of a myriad of inter connecting voids within non-collapsible structures with a large porous surface that can entrap wide range of actives (cosmetics, over-the-counter (OTC) skin care, sunscreens and prescription products). A typical 25 μm sphere can have up to 250000 pores and an internal pore structure equivalent to 10 ft in length providing a total pore volume of about 1ml/g. Microsponge technology offers entrapment of ingredients and is believed to contribute towards reduced side effects, increased efficacy, improved stability, increased elegance and enhanced formulation flexibility.[3,31,32] In addition, numerous studies have confirmed that microsponge systems are non- irritating, non- mutagenic, non-allergenic and non-toxic.

The microsponge drug delivery system (MDS) releases its active ingredient on a time mode and also in response to other stimuli (rubbing, temperature, pH, etc.) Microsponges have the capacity to absorb or load a high degree of active materials into the particle or onto its surface. Its large capacity for entrapment of actives up to 3 times its weight differentiates microsponges from other types of dermatological delivery systems. The MDS has advantages over other technologies like microencapsulation and liposomes. Microcapsules cannot usually control the release rate of actives. Once the wall is ruptured the actives contained within microcapsules will be released. Microsponges are stable over range of pH 1 to 11, temperature up to 130°C, compatible with most vehicles and ingredients, self sterilizing as average pore size is 0.25 μm where bacteria cannot penetrate, higher payload (50 to 60%), still free flowing and can be cost effective. Most liquid or soluble ingredients can be entrapped in the particles.

The Microsponges are prepared by different methods using emulsion systems as well as by suspension polymerization in a liquid–liquid system. The most common emulsion system used is oil-in-water (o/w), with the microsponges which are produced by the emulsion solvent diffusion method.[33]

II. MATERIAL AND METHODS

2.1 Analytical Method for Identification of Acyclovir

1. λ **max** by determination of UV spectroscopy.

2. Fourier transformed infrared spectrometry.

3.　　Differential Scanning Calorimetry. (DSC)

2.2　　Authentication of Drug

2.2.1　　λ $_{max}$ by determination of UV spectroscopy

➢　　**Preparation of stock solution**

10 mg of Acyclovir was accurately weighed and transformed to 100 ml clean and dry volumetric flask and 70 ml of solution (i.e. Ph 1.2, pH 6.8 and pH 7.4 phosphate buffer) and sonicate to dissolve the drug completely and make up the volume with same solvent (i.e, pH 1.2, pH 6.8 and pH 7.4 phosphate buffer).

➢　　**Preparation of Sub-stock solution**

Sub-stock solution of Acyclovir is prepared by taking aliquot from stock solution and dilute them using same solvent (i.e, pH 1.2, pH 6.8 and pH 7.4 Phosphate buffer). Take the absorbance at 301.8 nm, 330.8 nm and 330.0 nm, respectively.

➢　　**Preparation of calibration curve**

For the calibration curve of the Acyclovir standard stock solution and sub stock solution of Acyclovir was prepared in solution of different pH, pH 1.2, pH 6.8 and pH 7.4 Phosphate buffer and plot the graph between concentration v/s absorbance.

2.2.2　　Fourier transmission Infrared (FT-IR) Spectral analysis (Drug & Drug-exipient Compatibility study)

FTIR spectroscopy was performed on Fourier transformed infrared spectrophotometer (Jasco International) The pellets of drug and potassium bromide were prepared by compressing the powders at 20 psi for 10 mint on KBr press and the spectra were scanned in the wave number range of 600-4000 cm^{-1}. FTIR study was carried on Acyclovir.

➢　　**IR values of Acyclovir**

TABLE 1
IR VALUES OF ACYCLOVIR.

Functional Group Gro	Wave Number cm -1m^{-1})
O-H Stretching mode associated with the hydroxyl group	3600-3200
C-H stretch of the aromatic group	~3000
C = C stretch of the aromatic group; N-H bond scissoring	1619
C-C stretching mode	1449, 1490
O-H deformation of the hydroxyl groups	1355, 1378
In plane bending mode	1190- 1267
C-O stretching mode	1131
C-H bond Out of plane bending mode; ring deformation of the aromatic group	685-808

2.2.3　　Differential Scanning Calorimetry (DSC) studies

The sample of Acyclovir was scanned at 10˚C/min from 30˚C to 305˚C and thermal behavior of the drug was studied by recording the thermogram. The DSC thermogram of Acyclovir exhibited sharp endothermic peak. This is same as that of melting point of Acyclovir.

2.3　　Formulation of Acyclovir Microsponges

Microsponges were prepared by **Quasi Emulsion Solvent Diffusion Technique** which requires two immiscible phases internal and external phase with a surfactant which aids formation of an emulsion by reducing the interfacial tension.

2.4   Method of preparation of Acyclovir Microsponges using Eudragit RS-100 and Eudragit ES-100

The required amount of Acyclovir and Eudragit polymers were weighed accurately and dissolved in 20 ml of DCM: IPA (1:1) under sonication. The surfactant PVA was weighed accurately and dissolved in distilled water. The surfactant mixtures were allowed to cool to room temperature. The internal phase containing Acyclovir and Eudragit was added drop wise with the aid of syringe with stirring at 1500 rpm until the complete diffusion of the external phase i.e. about 8 hrs. After complete diffusion of the external phase the microsponges were filtered and dried overnight at room temperature.

2.5   Formulation Batches

TABLE 2
DIFFERENT BATCHES OF THE MICROSPONGE FORMULATIONS

SR No	Ingredients	Different Formulation Batches									
		MMS1	MMS2	MMS3	MMS4	MMS5	MMS6	MMS7	MMS8	MMS9	MMS10
1	Drug:Polymer ratio	1:1	1:1	1.5:1	1.5:1	2:1	2:1	2.5:1	2.51	3:1	3:1
	Internal Phase										
2	Acyclovir (mg)	500	500	750	750	1000	1000	1250	1250	1500	1500
3	Eud RS 100 (mg)	500	_	500	_	500	_	500	_	500	_
4	Eud ES 100 (mg)	_	500	_	500	_	500	_	500	_	500
5	Dichloromethane (DCM)	10	10	15	15	20	20	25	25	30	30
7	Iso-propyl Alcohol (ml)	10	10	15	15	20	20	25	25	30	30
8	Di-Butyl Pthalate (ml)	5	5	5	5	5	5	5	5	5	5
	External Phase										
9	PVA (mg)	50	50	75	75	100	100	125	125	150	150
10	Water (ml)	75	75	100	100	125	125	150	150	175	175

III.   RESULTS AND DISCUSSION

3.1   Construction of calibration curve by UV-Visible Spectrophotometer

3.1.1   Calibration curve of Acyclovir in HCL pH 1.2
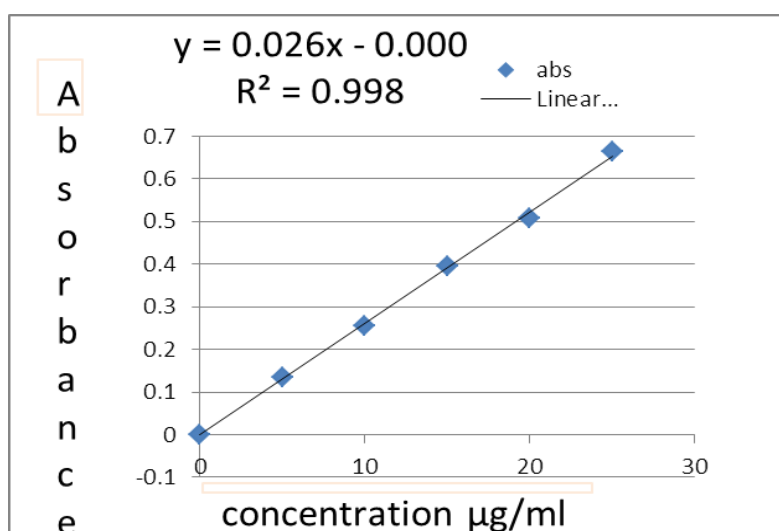
FIGURE 1: Calibration curve of Acyclovir in HCL pH 1.2.

3.1.2 Calibration curve of Acyclovir in PBS pH 6.8
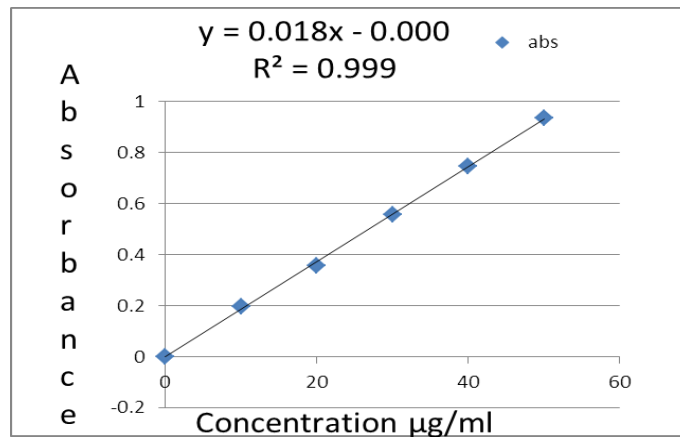
FIGURE 2: Calibration curve of Acyclovir in PBS pH 6.8.

3.1.3 Calibration curve of Acyclovir in PBS pH 7.4
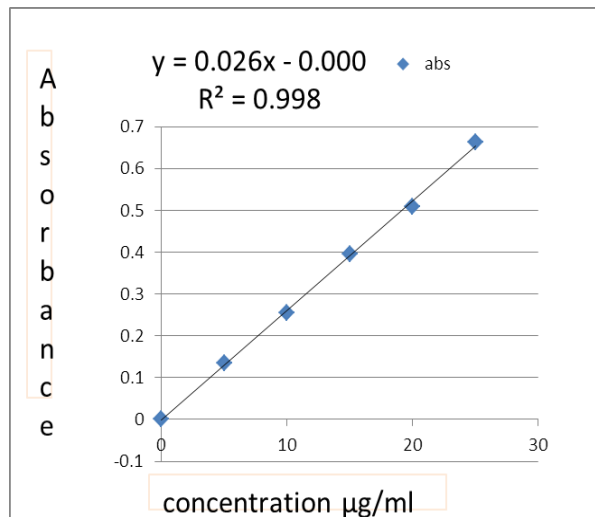
FIGURE 3: Calibration curve of Acyclovir in PBS pH 7.4.

3.1.4 Fourier transmission Infrared (FT-IR) Spectroscopy
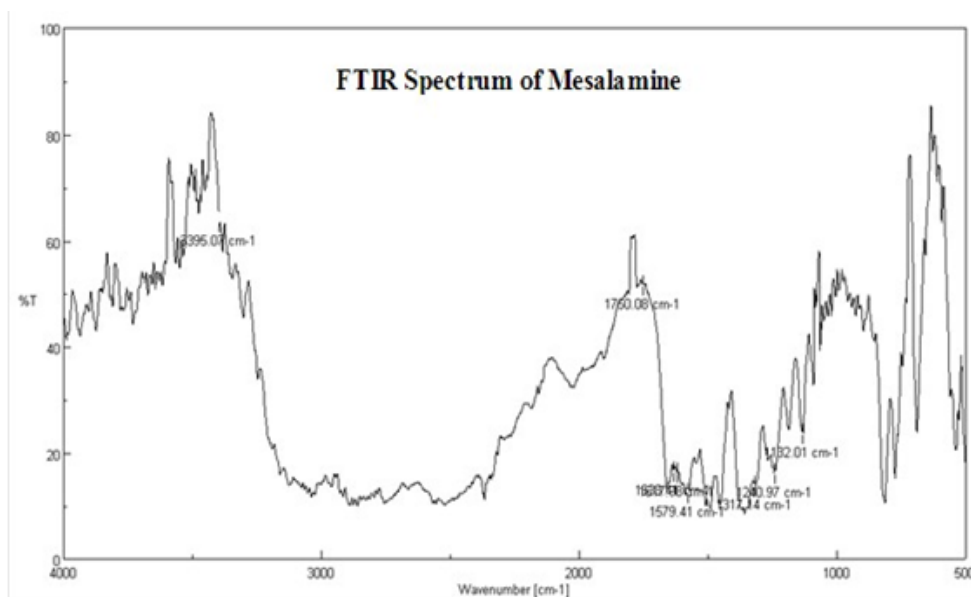
FIGURE 4: FTIR spectra of the Acyclovir.

3.1.5   Differential scanning colorimetry (DSC)
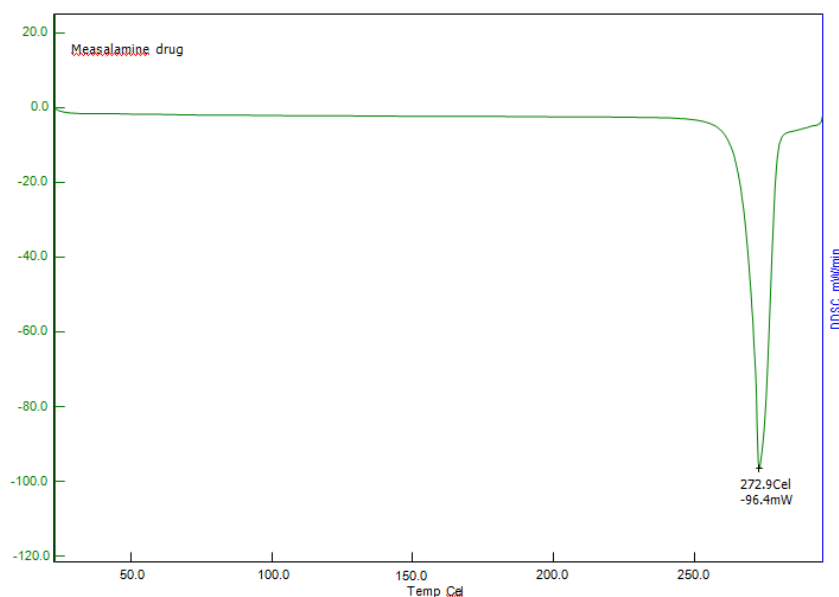
FIGURE 5: DSC plot of the Acyclovir.

3.1.6   Characterization of microsponges

TABLE 3
CHARACTERIZATION OF POWDERED MICROSPONGES.

Sr no	Formulation Code	Evaluation Parameters				
		Angle of Repose (θ)	Bulk Density (gm/cm3)	Tapped Density (gm/cm3)	Carr's Index (%)	Hausners Ratio
1	MMS1	23.75	0.51±0.01	0.57±0.01	11.86	1.11
2	MMS 2	24.46	0.52±0.01	0.55±0.02	12.00	1.09
3	MMS 3	25.20	0.51±0.01	0.53±0.01	10.53	1.12
4	MMS 4	25.24	0.52±0.01	0.57±0.01	11.48	1.13
5	MMS 5	25.35	0.52±0.01	0.59±0.01	11.53	1.16
6	MMS 6	23.56	0.50±0.01	0.57±0.01	11.80	1.10
7	MMS 7	24.35	0.52±0.01	0.55±0.02	12.05	1.09
8	MMS 8	25.18	0.50±0.01	0.53±0.01	11.15	1.11
9	MMS 9	25.45	0.52±0.01	0.57±0.01	11.42	1.10
10	MMS 10	25.38	0.53±0.01	0.59±0.01	11.55	1.13

3.1.7   Characterization of coated tablets [27]

TABLE 4
CHARACTERIZATION OF COATED TABLETS

Coated Tablets Of Batch MMS 5	Evaluation Parameters			
	Average Weight (mg)	Average Thickness (mm)	Hardness (Kg/cm^2)	Friability (%)
1	629.88	6.11	10.26	0.73
2	630.20	6.11	10.35	0.75
3	629.50	6.12	10.39	0.77
4	629.76	6.10	10.45	0.76
5	631.20	6.12	10.52	0.76
6	631.35	6.12	10.56	0.78

3.2 Trial Batches for the Selection of Drug as to polymer ratio

3.2.1 Selection of Drug: Polymer ratio in initial trials:

TABLE 5
SELECTION OF DRUG: POLYMER RATIO IN INITIAL TRIALS.

SR No	Ingredients	Different Formulation Batches									
		MMS1	MMS2	MMS3	MMS4	MMS5	MMS6	MMS7	MMS8	MMS9	MMS 10
1	Drug:Polymer ratio	1:1	1:1	1.5:1	1.5:1	2:1	2:1	2.5:1	2.5:1	3:1	3:1
	Internal Phase										
2	Acyclovir (mg)	500	500	750	750	1000	1000	1250	1250	1500	1500
3	Eud RS 100 (mg)	500	_	500	_	500	_	500	_	500	_
4	Eud ES 100 (mg)	_	500	_	500	_	500	_	500	500	500
5	Dichloromethane (DCM)	10	10	10	10	10	10	10	10	10	10
7	Iso-propyl Alcohol (ml)	10	10	10	10	10	10	10	10	10	10
8	Di-Butyl Pthalate (ml)	5	5	5	5	5	5	5	5	5	5
	External Phase										
9	PVA (mg)	100	100	100	100	100	100	100	100	100	100
10	Water (ml)	100	100	100	100	100	100	100	100	100	100

3.2.2 IN-VITRO drug release studies of Acyclovir loaded microsponges

In-vitro release studies were carried out in USP basket apparatus with stirringrate 50 rpm at $37\pm0.5^{\circ}$C. Initial drug release was carried out in 900 ml of 0.1 N hydrochloric acid for 2 hours followed by phosphate buffer pH 6.8 for next 2 hours followed by phosphate buffer PH 7.4 for next 8 hours. Samples were withdrawn at regular intervals and analyzed spectrophotometrically, at 301.8, 330.8, 330 nm respectively.

3.2.3 IN-VITRO drug release data for Eudragit RS-100 and ES-100 based colon specific

TABLE 6
DISSOLUTION READINGS OF THE FORMULATED BATCHES.

SR no	Media	Time (Hr)	% Cumulative Drug Release									
			MMS1	MMS2	MMS3	MMS4	MMS5	MMS6	MMS7	MMS8	MMS9	MMS10
			Eud RS 100	Eud ES 100	Eud RS 100	Eud ES 100	Eud RS 100	Eud ES 100	Eud RS 100	Eud ES 100	Eud RS 100	Eud ES 100
			1:1	1:1	1.5:1	1.5:1	2:1	2:1	2.5:1	2.5:1	3:1	3:1
1	HCL PH 1.2	1	0.02	0.034	0.0126	0.06	0.07	0.01	0.02	0.07	0.02	0.02
2		2	0.03	0.05	0.26	0.06	0.08	0.02	0.03	0.08	0.03	0.03
3	PBS PH 6.8	3	0.12	0.17	0.12	0.17	0.19	0.11	0.12	0.10	0.12	0.12
4		4	0.12	0.17	0.12	0.17	0.20	0.12	0.12	0.10	0.13	0.13
5	PBS PH 7.4	5	15.14	16.50	16.44	15.55	19.00	21.48	20.80	16.90	18.40	17.28
6		6	20.90	19.00	20.35	21.63	23.45	22.50	22.38	17.80	22.60	19.66
7		7	20.49	20.50	29.15	27.55	32.16	30.10	29.50	20.65	30.15	24.20
8		8	36.10	32.15	41.44	38.83	43.66	39.80	44.52	33.32	40.16	33.18
9		9	51.50	46.80	56.30	48.37	61.28	50.62	50.34	39.88	54.68	43.10
10		10	63.00	50.38	67.85	57.90	70.22	67.36	62.65	48.12	61.90	45.75
11		11	68.66	62.68	72.30	64.95	79.12	73.44	65.50	58.15	62.12	57.40
12		12	77.50	71.65	78.30	74.15	84.50	82.40	75.26	72.20	72.28	68.35

3.3   Results

Total 10 formulation were formulated MMS 1- MMS 10. The formulation batches **MMS 5** and **MMS 6** shows highest drug release, 84.50 and 82.40% respectively, having the Drug: Polymer ratio of **2:1**

3.3.1   Selection of Internal Phase for the Formulation of Microsponges

TABLE 7
SELECTION OF INTERNAL PHASE.

SR No.	Concentration of Polymer in Internal phase (mg)		Formation of Microsponges		Physical Appearance of microsponges		Particle Size (in µm)	
	RS 100	ES100	RS 100	ES 100	RS 100	ES 100	RS 100	ES 100
1	300	300	+	+	Irregular Spherical	Irregular Spherical	14.28	16.25
2	350	350	+	+	Spherical	Spherical	14.83	16.56
3	400	400	+	+	Spherical	Spherical	15.56	17.25
4	450	450	+	+	Spherical	Spherical	16.52	19.18
5	**500**	**500**	+	+	**Spherical**	**Spherical**	16.99	20.0
6	550	550	+	+	Irregular	Irregular	17.35	21.88
7	600	600	+	+	Spherical microsponges which Collapses after some time	Irregular microsponges	19.60	24.17
8	650	650	+	+	Spherical	Spherical microsponges which Collapses after some time	28.25	30.46
9	700	700	+	+	Spherical	Spherical	33.16	533.89
10	750	750	+	+	Spherical Rigid	Spherical Rigid	35.80	36.42

3.3.2   Selection of Concentration of Polymer in the Internal Phase

TABLE 8
SELECTION OF CONCENTRATION OF POLYMER IN THE INTERNAL PHASE.

SR NO	DRUG:POLYMER RATIO	INTERNAL PHASE (ml)	EXTERNAL PHASE (ml)	PVA (mg)	DRUG CONTENT (%)		FREE DRUG CONTENT (%)		% ENTRAPMENT	
					RS 100	ES 100	RS 100	ES 100	RS 100	ES 100
1	1:1	20●	125	100	32.42	30.14	27.80	28.26	20.42	19.25
2	1:1	20▲	125	100	36.64	35.90	10.70	10.89	33.94	32.3
3	1:1	20*	125	100	28.75	27.09	32.65	32.20	17.15	16.1
4	1:1	20♦	125	100	36.48	35.55	9.86	10.85	35.32	34.5
5	1:1	20▲●	125	100	52.60	52.10	12.90	13.15	72.70	71.60
6	**1:1**	**20♦▲**	**125**	**100**	**65.75**	**65.00**	**5.10**	**5.68**	**83.02**	**80.47**
7	1:1	20♦●	125	100	36.48	35.35	9.56	10.85	35.32	34.50
8	1:1	20▲*	125	100	41.87	40.56	12.22	13.15	28.67	28.30
9	1:1	20♦*	125	100	50.15	49.35	15.7	17.8	29.3	25.75
10	1:1	20●*	125	100	18.30	17.38	22.00	22.45	25.6	24.10

*●Ethanol, ▲ Dichloromethane, ♦ IPA, * Methanol*

3.3.3   Selection of Surfactant Concentration in the External Phase:

TABLE 9
SELECTION OF SURFACTANT CONCENTRATION IN THE EXTERNAL PHASE

S. No	Drug: Polymer	PVA (mg)	External phase (Water) (ml)	Physical appearance		Particle Size in µm		Drug Content (%)		Free Drug Content (%)		% Entrapment	
				RS 100	ES100	RS 100	ES 100	RS 100	ES100	RS 100	ES 100	RS 100	ES 100
1	2:1	50	125	Large Clumps	Large Clumps	-	-	-	-	-	-	-	-
2	2:1	75	125	Irregular Large	Irregular Large	16.86	18.56	35.50	32.22	7.30	8.60	81.50	80.20
3	**2:1**	**100**	**125**	**Uniform Spherical Rigid**	**Uniform Spherical**	16.99	20.0	**65.75**	**65.00**	**5.10**	**5.68**	**83.02**	**80.47**
4	2:1	125	125	Uniform Spherical Rigid	Uniform Spherical Rigid	20.25	22.39	65.47	65.22	6.15	6.11	82.88	80.15
5	2:1	150	125	Uniform Spherical Rigid	Uniform Spherical Rigid	21.56	24.67	63.20	62.11	7.50	7.92	80.50	79.45
6	2:1	175	125	Uniform Spherical Rigid	Uniform Spherical Rigid	25.22	29.32	62.4	62.05	7.90	8.30	77.45	76.65
7	2:1	200	125	Uniform Spherical Rigid	Uniform Spherical Rigid	27.46	31.28	59.88	59.65	7.70	8.48	73.90	72.55
8	2:1	225	125	Uniform Spherical Rigid	Uniform Spherical Rigid	27.98	29.54	58.36	58.21	10.50	11.26	70.45	70.12
9	2:1	250	125	Irregular Big	Irregular Big	30.75	32.22	55.84	55.36	13.55	15.30	68.05	67.00
10	2:1	275	125	Irregular Big	Irregular Big	33.16	34.57	52..2	51.56	16.60	17.11	64.80	60.50

3.3.4   Effect of External Phase Volume on Microsponge

TABLE 10
EFFECT OF EXTERNAL PHASE VOLUME ON MICROSPONGE.

SR No	External phase (ml)	PVA(mg)	Physical appearance		Particle Size in μm		Drug Content (%)		Free Drug Content (%)		% Entrapment	
			RS 100	ES100	RS 100	ES100	RS 100	ES100	RS 100	ES100	RS 100	ES 100
1	75	100	Irregular	Irregular	34.12	35.36	45.76	42.83	9.10	11.5	47.60	44.10
2	100	100	Spherical	Spherical	32.62	34.91	51.53	48.20	5.60	5.85	61.83	58.48
3	**125**	**100**	**Spherical**	**Spherical**	16.99	20.0	**65.75**	**65.00**	**5.10**	**5.68**	**83.02**	**80.47**
4	150	100	Spherical Uniform	Spherical Uniform	15.56	17.25	65.05	62.40	4.30	4.82	79.16	81.10
5	175	100	Spherical Uniform	Spherical Uniform	15.35	16.86	63.90	60.20	7.65	8.38	66.50	69.5
6	200	100	Spherical Uniform	Spherical Uniform	14.92	15.48	60.32	56.30	10.30	11.5	56.60	55.74
7	225	100	Spherical Uniform	Spherical Uniform	13.56	13.98	57.43	52.45	15.50	17.2	50.25	48.55
8	250	100	Irregular Shape	Irregular shape	12.67	13.32	53.90	48.60	17.22	20.5	48.20	36.82
9	275	100	Irregular Nonuniform	Non-Uniform	12.56	13.12	48..20	42.78	18.60	23.1	37.90	33.15
10	300	100	Irregular Large size	Irregular Large size	12.15	12.63	44.56	40.88	19.95	25.8	33.88	29.40

3.3.5   Effect of Internal Phase Volume on Microsponges

TABLE 11
EFFECT OF INTERNAL PHASE VOLUME ON MICROSPONGES.

SR No.	Internal phase (ml)	Particle Size (in μm)		Drug Content (%)		Free Drug Content (%)		% Entrapment	
		RS 100	ES 100	RS 100	ES 100	RS 100	ES 100	RS 100	ES 100
1	10.00	32.10	33.55	47.61	45.76	9.10	11.5	47.60	44.10
2	15.00	31.53	32.65	51.53	47.07	5.60	5.85	58.48	55.50
3	**20.00**	16.99	20.0	**65.75**	**65.00**	**5.10**	**5.68**	**83.02**	**80.47**
4	25.00	16.24	17.36	62.23	60.45	4.25	5.15	82.14	78.89
5	30.00	**15.35**	**16.58**	60.95	58.20	10.60	9.23	79.00	74.20

3.3.6   Effect of Rate of Stirring on Microsponges

TABLE 12
EFFECT OF RATE OF STIRRING ON MICROSPONGES.

SR No	Stirring in rpm (For 8 Hrs)	Physical Appearance		Mean Particle Size in μm		Drug Content (%)		Free Drug Content (%)		% Entrapment	
		RS 100	ES 100	RS 100	ES 100	RS 100	ES 100	RS 100	ES100	RS 100	ES 100
1	500	-	-	-	-	-	-	-	-	-	-
2	800	Irregular large	Irregular	98	109	61.30	58.65	5.50	5.65	65.10	64.20
3	1000	Spherical	Spherical	65	78	63.53	61.12	4.10	4.55	70.49	67.50
4	1200	Uniform Spherical	Uniform Spherical	35.98	39.40	65.47	65.22	2.95	2.78	75.16	71.10
5	**1500**	**Uniform Spherical**	**Uniform Spherical**	16.99	20.0	**65.75**	**65.00**	**5.10**	**5.68**	**83.02**	**80.47**
6	1700	Uniform Spherical	Uniform Spherical	15.56	17.25	65.47	65.22	3.65	3.98	79.16	77.10
7	1900	Uniform Spherical	Uniform Spherical	15.35	16.86	59.88	59.45	5.75	6.05	62.25	59.40
8	2000	Uniform Spherical	Uniform Spherical	14.92	15.48	57.36	58.11	6.70	7.11	56.20	54.80
9	2500	Uniform Spherical	Uniform Spherical	13.56	13.98	54.80	55.46	8.09	10.95	45.55	43.20
10	3000	Uniform Spherical	Uniform Spherical	12.67	13.32	50..25	50.50	11.02	13.45	43.26	42.50

3.3.7   Effect of Stirring Time on the Formation of Microsponge

TABLE 13
EFFECT OF TIME OF STIRRING ON MICROSPONGES.

S No	Drug / Polymer	Time of Stirring in Hrs (at 1500 rpm)	Physical Appearance		Particle Size		Drug Content (%)		Free Drug Content (%)		% Entrapment	
			RS 100	ES 100i	RS 100	ES 100	RS 100	ES 100	RS 100	ES 100	RS 100	ES 100
1	2:1	1	Suspension filtered as such	Suspension filtered as such	-	-	-	-	-	-	-	-
2	2:1	2	Suspension filtered as such	Suspension filtered as such	-	-	-	-	-	-	-	-
3	2:1	4	irregular shape	irregular shape	45.25	48.80	58.50	55.12	8.10	9.55	65.49	62.50
4	2:1	6	spherical	spherical	32.68	35.00	65.47	65.22	2.95	2.78	75.16	71.10
5	2:1	8	spherical rigid	spherical rigid	16.99	20.0	65.75	65.00	5.10	5.68	83.02	80.47
6	**2:1**	**10**	**spherical rigid**	**spherical rigid**	**15.30**	**55.86**	**66.47**	**64.22**	**4.85**	**5.26**	**83.85**	**81.80**

3.3.8　Effect of Drug / Polymer Ratio on Physical Properties of Microsponges

TABLE 14
EFFECT OF DRUG / POLYMER RATIO ON PHYSICAL PROPERTIES OF THE MICROSPONGES

SR No	Drug: Polymer	Production Yield (%)		Mean Particle Size in μm		Drug Content (%)		Free Drug Content (%)		% Entrapment	
		RS100	ES 100	RS 100	ES 100	RS 100	ES 100	RS 100	ES100	RS 100	ES 100
1	1:1	49.52	47.80	32.00	33.42	47.61	45.76	13.68	15.80	47.60	45.94
2	1.5:1	67.92	67.54	31.53	32.65	51.53	47.07	7.60	9.85	61.83	56.17
3	2:1	78.00	77.37	16.99	20.0	65.75	65.00	5.10	5.68	83.02	80.47
4	2.5:1	84.48	86.56	16.24	17.36	66.53	64.23	5.25	5.69	85.48	83.39
5	**3:1**	**89.30**	**88.32**	**15.37**	**16.20**	**67.46**	**65.84**	**4.43**	**5.05**	**86.34**	**83.91**

3.4　In-Vitro Drug Release Studies[18,26]

3.4.1　IN-VITRO drug release studies of Acyclovir loaded microsponges

In-vitro release studies were carried out in USP basket apparatus with stirring rate 50 rpm at 37 ± 0.5^{o}C. Initial drug release was carried out in 900 ml of 0.1 N hydrochloric acid for 2 hours followed by phosphate buffer pH 6.8 for next 2 hours followed by phosphate buffer PH 7.4 for next 8 hours. Samples were withdrawn at regular intervals and analyzed spectrophotometrically, at 301.8, 330.8, 330 nm respectively.

3.4.2   IN-VITRO drug release data for Eudragit RS-100 and ES-100 based colon specific formulations

TABLE 15
DISSOLUTION READINGS OF THE FORMULATED BATCHES.

SR no	Medium	Time (Hr)	% Cumulative Drug Release									
			MMS1	MMS2	MMS3	MMS4	MMS5	MMS6	MMS7	MMS8	MMS9	MMS10
			Eud RS 100	Eud ES 100	Eud RS 100	Eud ES 100	Eud RS 100	Eud ES 100	Eud RS 100	Eud ES 100	Eud RS 100	Eud ES 100
			1:1	1:1	1.5:1	1.5:1	2:1	2:1	2.5:1	2.5:1	3:1	3:1
1	HCL PH 1.2	1	0.02	0.034	0.0126	0.06	0.07	0.01	0.02	0.07	0.02	0.02
2		2	0.03	0.05	0.26	0.06	0.08	0.02	0.03	0.08	0.03	0.03
3	PBS PH 6.8	3	0.12	0.17	0.11	0.17	0.19	0.10	0.12	0.015	0.12	0.12
4		4	0.12	0.17	0.13	0.17	0.20	0.12	0.13	0.10	0.12	0.12
5	PBS PH 7.4	5	15.14	15.09	17.44	17.80	19.60	21.48	24.83	21.76	20.10	19.22
6		6	20.90	18.07	21.25	22.30	26.33	23.63	24.52	27.82	24.30	23.48
7		7	20.49	22.40	28.09	25.88	36.76	33.95	33.14	35.90	32.99	33.60
8		8	36.19	34.17	41.44	39.38	45.69	39.23	48.92	39.55	43.45	38.66
9		9	52.79	50.33	59.60	48.35	69.88	51.46	61.88	56.49	62.52	43.40
10		10	65.46	52.42	70.28	57.90	67.81	66.15	70.20	60.44	68.88	56.10
11		11	76.06	64.98	79.30	68.95	83.81	75.55	78.72	67.46	75.15	64.98
12		12	79.90	73.43	81.88	79.10	92.12	87.82	83.26	75.35	79.40	71.99

3.5　　Results

Total 10 formulation were formulated MMS 1- MMS 10. The formulation **MMS 5** shows highest drug release, 92.12%.

3.6　　STABILITY STUDIES [25,30]

Stability studies of the developed formulations were carried out according to ICH and WHO guidelines. The formulations MMS 1- MMS 10 sealed in aluminum foils were kept in the stability chamber maintained at 40^0 C $\pm$ 2^0C and 75% $\pm$ 5% RH for 3 months. The samples were analyzed for the drug content for 2 month period (ie- 60 days study).

Stability data is presented in Table.

3.7　　Stability studies of different formulations. Mean ± S.D. Dissolution study of all the batches

TABLE 16
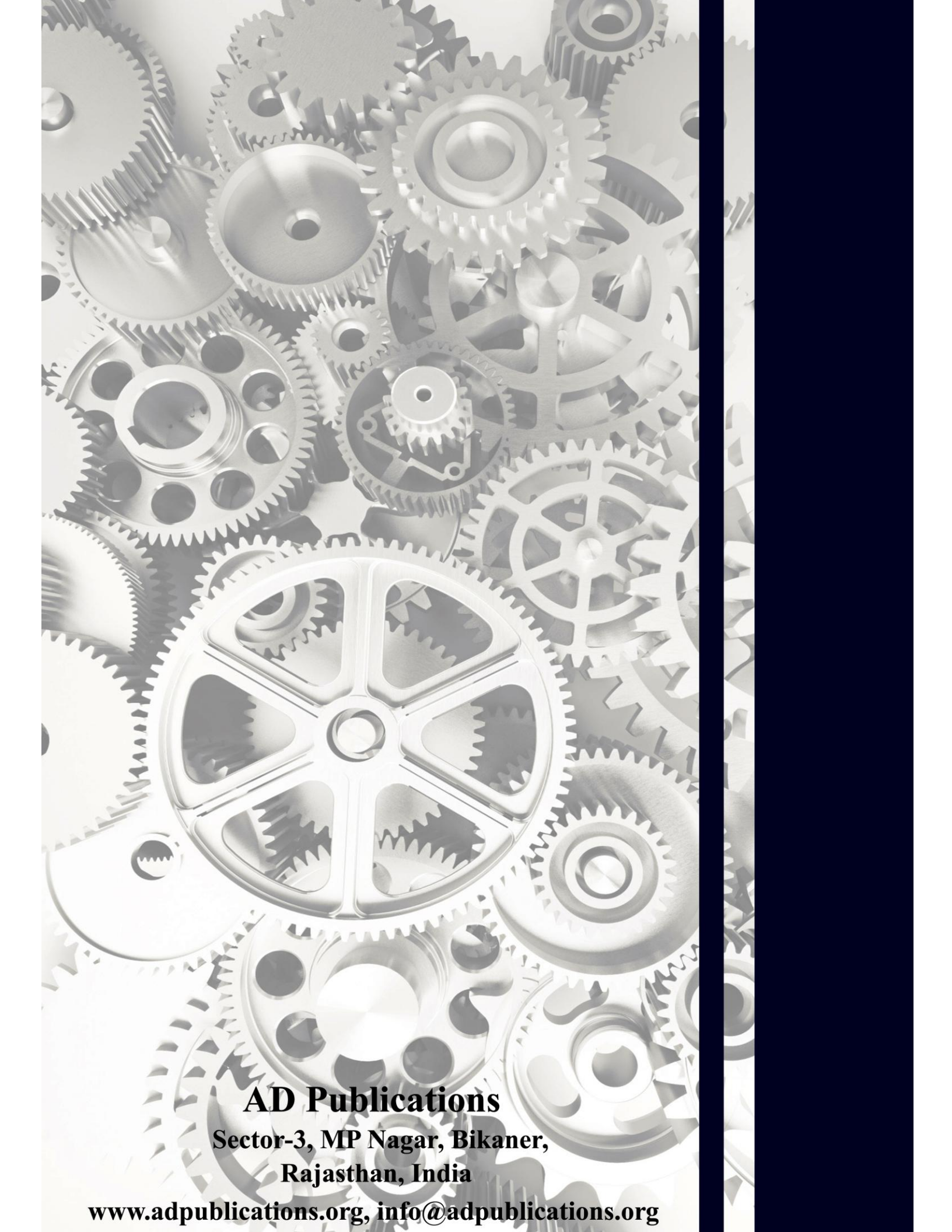**STABILTY STUDY DATA OF THE ALL BATCHES FOR TWO MONTH.**

SR NO.	FORMULATION CODE	DRUG CONTENT (%)	
		AFTER 30 DAYS	AFTER 60 DAYS
		ACYCLOVIR	ACYCLOVIR
1	MMS 1	79.71	79.54
2	MMS 2	73.35	73.20
3	**MMS 3**	**81.68**	**81.56**
4	MMS 4	79.00	78.92
5	MMS 5	92.08	92.00
6	MMS 6	87.74	87.65
7	MMS 7	83.20	83.05
8	MMS 8	75.15	75.00
9	MMS 9	79.30	79.19
10	MMS 10	71.90	71.76

IV.　　CONCLUSION

1) Microsponge containing Acyclovir was prepared by Quasi-emulsion diffusion method using Eudragit RS 100 and ES100 polymers.

2) All the microsponge formulations were subjected for the drug content estimation and loading efficiency. The drug content was uniform and reproducible in all the formulations.

3) The **IR spectral analysis** suggested that there were no interaction between the drug and formulation additives.

4) **Internal Phase Volume:** As there is increase in the internal phase volume, there is decrease in the Particle Size, Drug Content and Entrapment Efficiency and there is Increase in the free drug content.

5) **Polymer Concentration:** As Polymer concentration increases, the drug release decreases.

6) **Surfactant Concentration:** As surfactant concentration increases, there is increase in the particle size and, decrease in the encapsulation efficiency and the production yield and larger microsponges.

7) **External Phase Volume:** As there is increase in the external phase volume, there is decrease in drug content, drug entrapment and increase in the free drug content and particle size.

8) **Rate of stirring:** As stirring speed increases there is increase in the free drug content and there is decrease in the drug content, entrapment efficiency and particle size.

9) **Time of stirring:** As stirring time increases there is decrease in the free drug content, particle size and there is increase in the entrapment efficiency and drug content.

10) **Drug: Polymer Ratio:** As there is increase in the drug: polymer ratio, there is increase in the encapsulation efficiency and the production yield, decrease in the particle size.

11) The dissolution was carried out of all the batches.

REFERENCES

[1] Raymond C R, Sheskey P J and Marian E Q., Editors. Handbook of Pharmaceutical Excipients, 6th edition 2006 Pharmaceutical Press and the American Pharmacists Association.

[2] Vyas SP, Khar RK, Targeted and Controlled Drug Delivery-Novel Carrier System: New Delhi: CBS Publication, 2002; 453-95.

[3] Kawashima Y, Niwa T, Handa T, Takeuchi H, Iwamoto T, Itoh K., Preparation of controlled-release microspheres of ibuprofen with acrylic polymer by a novel quasi- emulsion solvent diffusion method. J Pharm Sci., 1989; 78: 68-72.

[4] Perumal D., Microencapsulation of ibuprofen and Eudragit RS 100 by the emulsion solvent diffusion technique. Int. J. Pharm., 2001; 218: 1-11.

[5] Mandal TK, Bostanian LA, Graves RA, Chapman SR, Idodo TU., Porous biodegradable microparticles for delivery of Pentamidine. European Journal of Pharmaceutics and Biopharmaceutics, 2001; 52: 91-96.

[6] Tansel C. Nursin G, Tamer B., The effects of pressure and direct compression on tabletting of microsponges. Int. J. Pharm., 2002; 242: 191–95.

[7] Beruto DT, Botter R, Fini M., The effect of water in inorganic microsponges of calcium phosphates on porosity and permeability of composites made with polymethylmethacrylate. Biomaterials., 2002; 23: 2509-17.

[8] Tansel Comoglu, Nursin Gonul, Tamer Baykara., Preparation and in vitro evaluation of modified release ketoprofen microsponges. II Farmaco, 2003; 58: 101-106.

[9] Kilicarslan M, Baykara T., The effect of drug/polymer ratio on the properties of the Verapamil Hydrochloride loaded microspheres. Int. J. Pharm., 2003; 252: 99-109.

[10] United state Pharmacopoeia 32 and National Formulary, 2009; 27(III): 2894.

[11] Orlu M, Cevher E and Araman A., Design and evaluation of colon specific drug delivery system containing flurbiprofen microsponges. Int. J. Pharm., 2006; 318: 103-17.

[12] British Pharmacopoeia, 2009; II: 1311-1313.

[13] Chadavar V and Shaji J., Microsponge Delivery System. Current Drug Delivery., 2007; 4: 123-29.

[14] Patel G, Patel JK. Use of a Microsponge in Drug Delivery Systems. Available from. Kilicarslan M, Baykara T. The effect of the drug/polymer ratio on the properties of Verapamil HCl loaded microspheres. Int J Pharm, 2003; 252: 99-109.

[15] American journal of pharmatech research. Microsponge Drug Delivery System: A novel dosage form Rahul Shivali Patil 1, Vishnu uddhav kemar 2, s.s. patil 1. Ashokraomane college of pharmacy, peth-vadgaon. Ichalkaranji, Kolhapur, MS.2 Appasaheb Birnale college of pharmacy, south shivaji nagar, sangali, MS.

[16] Microsponges for colon targeted drug delivery system: an overview rajendra jangde*issn- 2231–5705 (print) issn- 2231–5713 (online) university institute of pharmacy, pt. ravishankar shukla university, raipur.

[17] USP dissolution medium database; updated feb 2016.

[18] Martin A, Swarbrick J, Cammarrata A. (1991) Chapter 19, In: Physical Pharmacy- Physical Chemical Principles in Pharmaceutical Sciences. 3rd Ed., pp 527.

[19] Acyclovir [Internet] 2009 (UPDATED 2011 Jan 27) Available from: http://en.wikipedia.org/wiki/Acyclovir.

[20] http://www.drugs.com/drug-interactions/Acyclovir.html.

[21] Raymond C R, Sheskey P J and Marian E Q., Editors. Handbook of Pharmaceutical Excipients, 6th edition 2006 Pharmaceutical Press and the American Pharmacists Association